Upscaled models for two-phase flow in porous media with evolving interfaces at the pore scale

S. Sharmin, C. Bringedal, I.S. Pop

UHasselt Computational Mathematics Preprint
Nr. UP-20-01

Jan. 6, 2020

Upscaled models for two-phase flow in porous media with evolving interfaces at the pore scale

Sohely Sharmin[a,*], Carina Bringedal[b], Iuliu Sorin Pop[a]

[a] *Hasselt University, Campus Diepenbeek, Agoralaan Gebouw D, 3590 Diepenbeek, Belgium*
[b] *University of Stuttgart, Pfaffenwaldring 5a, 70569 Stuttgart, Germany*

Abstract. The modelling and simulation of the unsaturated flow or the flow of two immiscible fluid phases in a porous medium is challenging as this flow takes place through the pores of the medium, which form a highly complex domain. Next to the complexity of the domain, a major challenge is to account for the interface separating the fluids, or the unsaturated fluid from the inert filling part, as the location of this interface is not known a-priori. The evolution of this interface depends on the flow of both fluids and of the surface tension. Moreover, the surface tension may depend on the concentration of a surfactant dissolved in one fluid phase. In this work, such aspects are taken into account, and effective, Darcy-scale models are derived based on the known physics at the pore scale. In this sense a thin strip is used as the representation of a single pore in the porous medium. The Darcy-scale models are derived for various regimes, accounting for different pore-scale processes. Numerical examples show that the upscaled models are a good approximation of the transversal average of the solution to the pore-scale models, as the ratio of the width and the length of the pore approaches zero.
Keywords: Two-phase flow Freely moving interface Upscaled models Marangoni effect Capillary effect

1. Introduction

Two-phase flow in porous media is relevant for many industrial and environmental applications such as geological CO_2 sequestration, or oil recovery. Common for all these applications is the need to describe the flow at the Darcy scale (from now on the macro scale), the preferred scale for numerical simulations, where the grain and void space and the two (or more) fluid phases cannot be explicitly separated, but modelled through average quantities such as porosity and saturation. At the Darcy scale, the flow of each fluid phase is described with the help of Darcy-scale quantities like the absolute permeability, which depends strictly on the medium, and the fluid-specific relative permeability, which is a function of the fluid saturation.

The two-phase or, more general, the multi-phase and multi-component flow through a porous medium is inherently a process occurring at multiple scales, in which the processes at the pore scale do affect the overall flow on the Darcy scale. When considering the process at the scale of pores (here and below the micro scale), the fluids are assumed immiscible and they are separated by a fluid-fluid interface. The location of this interface gives directly the volume occupied by each of the two fluids within one pore, so it can be related directly to the saturation of the two fluids. The interface is evolving in an a-priori unknown manner, depending on the velocities of the two fluids and on the surface tension. This evolution has a high impact

*Corresponding author
Email address: sohely.sharmin@uhasselt.be (Sohely Sharmin)

on the overall flow behaviour. Simply knowing the saturation of the two fluids is not sufficient for describing the overall flow behaviour. We need to understand the processes affecting the fluid-fluid interface to be able to describe the flow.

One of the first mathematical models for the Darcy-scale flow in a porous medium was formulated by Henry Darcy [1], based on experiments. In these experiments only one fluid phase was considered, occupying the entire pore space so the porous medium was fully saturated. The experiments showed a proportionality between the pressure gradient and the flow rate. Subsequent extensions, still based on experimental observations, have considered unsaturated media [2], two-phase flow [3], or reactive transport [4] in porous media. Traditionally, the flow models involve the mass balance for each phase, the Darcy law with a saturation-dependent (relative) permeability, and that the phase-pressure difference (the capillary pressure) is a nonlinear, monotone function of the saturation of the (say) wetting fluid. The relative permeability functions, and the one for the capillary pressure, are determined experimentally.

Although extensively used such models need improvements, as also motivated by experimental results. As shown in [3], the capillary pressure - saturation function also depends on the process (infiltration or drainage). Also, the break-through curves determined in [5] for the phase-pressure difference, respectively for the saturation, reveal that the dependency of the former quantity on the latter is not necessarily monotone. Next to this, there is indirect evidence of the limited validity of assuming a nonlinear relationship dependency of the capillary pressure and the saturation. In this respect we mention that effects like saturation overshoot or finger formation, clearly evidenced in experiments reported e.g. in [6, 7, 8, 9] and [10, 11], are ruled out by the mathematical models used traditionally.

To overcome these drawbacks, extensions of Darcy's law for unsaturated or two-phase flow in porous media have been proposed. In this sense we start by mentioning [12, 13, 14, 15, 16], where different play-type hysteresis models are being proposed (an overview is provided in [17]), and [14, 18] for models incorporating dynamic effects in the capillary pressure - saturation dependency. Inspired by the thin film model proposed in [19], a phase-field model involving the second-order spatial derivative of the saturation in the capillary pressure is proposed in [20, 21] for unsaturated flow in porous media (also see [22]). Finally, in [23] a model accounting for the differences between percolating and non-percolating parts of a fluid is discussed, whereas the interfacial area concept is incorporated in the porous media flow models discussed in [24, 25, 26].

The effectiveness of such extensions in capturing phenomena like saturation overshoot and fingering is evidenced in [9, 21, 27, 28, 29, 30, 31, 32, 33, 34]. Two different major strategies can be observed in these papers. The first is to present numerical simulations for the extended models, aiming to reproduce the experimental results quantitatively. The second relies on mathematical analysis, and in particular on travelling waves, the focus being mainly on the qualitative behaviour of the solution, and in particular the dependence on the parameters appearing in the extended models.

The extended models discussed above are stated at the Darcy scale, where no distinction is being made between the pore space, wherethrough fluid flow takes place. These models are describing the averaged behaviour of the system by considering so-called representative elementary volumes, and without focussing on the detailed description of the processes inside each pore. Alternatively, one can consider the mathematical models valid at the scale of pores, which leads to models posed in an extremely complex domain consisting of the entire pore space of the porous medium. Although a numerical simulation at such detailed level is simply infeasible for practical applications, such an approach allows to incorporate detailed pore-scale physics, which is generally better understood (see e.g. [35, 36, 37, 38]). To overcome the difficulties related to the complexity of the domain, one can apply upscaling techniques to derive Darcy-scale models. Such an approach is adopted in [39, 40], by considering a simple pore geometry consisting of a long and thin pore, and for which transversal averaging is applied to derive a Darcy scale model. In this way, various model components and features can be included in a quite straightforward manner, and the corresponding Darcy-scale models can be derived in

a rational manner.

Here we follow the same approach for deriving Darcy-scale models for two-phase or unsaturated, one-phase flow in porous media. In the former case a wetting and a non-wetting fluid are present, in the latter only a wetting fluid is present together with a fluid that has constant pressure (say, zero) and infinite mobility. The fluids are assumed incompressible and immiscible. The derived models also take into account the possibility that one fluid is transporting a solute, which has an impact on the surface tension coefficient. We start with formulating the relevant models at the pore scale and then derive upscaled (Darcy-scale) models based on reasonable assumptions on the underlying physics.

At the pore scale we assume that the flow of each fluid phase is modelled by the Navier-Stokes equations. When referring to two fluid phases (the unsaturated, one-phase case being similar), a peculiar aspect in this approach is in the fact that, since the fluids are assumed immiscible, at the pore scale they are separated by an interface having a location that is not known a-priori. This interface moves depending on the fluid velocities, and, if applicable, on the concentration of the solute at this interface. In mathematical terms, this interface represents a free boundary in the model. Jump conditions ensuring conservation of the involved quantities are used at the evolving interface, as well as kinematic conditions to model its evolution.

To simplify the presentation, here we consider a single pore as a representative for the porous medium. In this case, the interface separating the two fluid phases can be seen as the thickness of the wetting phase layer. For more complicated situations, one can use e.g. a level set [41] approach. Alternatively, a diffuse interface approach can be considered, using e.g. the phase-field models in [42].

In any of these approaches, the resulting models can be used for deriving the upscaled, Darcy scale counterparts, which are more suited for numerical simulations. For the simplified situation here, we apply asymptotic expansion techniques and transversal averaging to derive the upscaled mathematical models. In doing so, we also include a solute-dependent surface tension, leading to so-called Marangoni effects in the upscaled equations.

This work is builds on [39, 40], where mathematically rigorous upscaling results are obtained for two-phase flow in a single pore. Compared to [39, 40], here we consider more regimes with respect to the capillary number, and also include solute effects in the surface tension dependency. We also mention that, although not considering the flow in a porous medium, in [43] a similar approach is used for deriving the shallow-water equations.

In this context, we mention that asymptotic homogenization methods in either a thin strip or in a periodic porous medium have been widely applied for many application in which evolving interfaces are encountered at the pore scale. Examples in this sense are the evolving fluid-solid interface due to mineral precipitation and dissolution [44, 45, 46, 47, 48, 49, 50], or to biofilm growth or other biological processes [51, 52, 53, 54, 55, 56, 57]. In all these cases, the derived Darcy-scale models were resembling well many of the models that are commonly accepted in the literature, but allow integrating additional effects in a rational manner.

The paper is organized as follows. In the next section the physical processes at the pore-scale and the corresponding mathematical models are introduced. With ϵ being a small parameter representing the ratio of the pore width and length, in Section 3, the pore-scale models are non-dimensionalized and their dependence on ϵ is derived. In Section 4 asymptotic expansion methods are applied to the pore-scale models and for various scaling regimes, and the corresponding upscaled are derived. In this sense, the cases in which the Marangoni effects do play a role at the Darcy scale are evidenced. Also, cases where the two upscaled fluid pressures are equal, or where the capillary pressure depends on the saturation in a non-standard way, resembling the models in [20, 21, 40, 39]. The results are summarized and discussed more closely in Section 5. Finally, Section 6 provides some numerical examples that confirm the validity of the approach. Specifically, the numerical solutions to the original, pore-scale models are computed for different situations, and then

their transversal averages are compared to the solutions to the upscaled models. These results demonstrate that, as ϵ approaches zero, the upscaled models are describing well the averaged behaviour of the pore-scale models, showing that the simplified, Darcy-scale models are a valid approximation of the pore-scale ones.

2. Mathematical model

A pore-scale model is considered for two-phase or unsaturated flow through a porous medium. For simplicity, we considered a thin two-dimensional strip to represent the local pore geometry. Two incompressible and immiscible fluids, where one is wetting and the other is non-wetting, are flowing through the strip. Densities and viscosities of the fluids are constant. The wetting phase is attached to the pore wall and the wetting layer has a thickness that changes with time and varies with the location of the wall. The two fluids are separated by a sharp interface with zero thickness which is changing with time. The movement is not known a-priori, hence we have a moving boundary at the fluid-fluid interface. The interface that separates the fluids moves because of the surface tension and of the flow/movement of the two fluids. There is a solute present only in the wetting fluid and the concentration of the solute will change subject to diffusion and transport. The surface tension is considered as a function of the solute concentration, which results in a tangential stress at the moving interface which is called the Marangoni stress. The gravity effects are neglected.

2.1. Geometric settings

The width and length of the thin strip are respectively $2\,l$ and L with $L >> l$. For simplicity, we assume a symmetric case with respect to (w.r.t.) the x-axis. The lower half of the strip is shown in Figure 1.

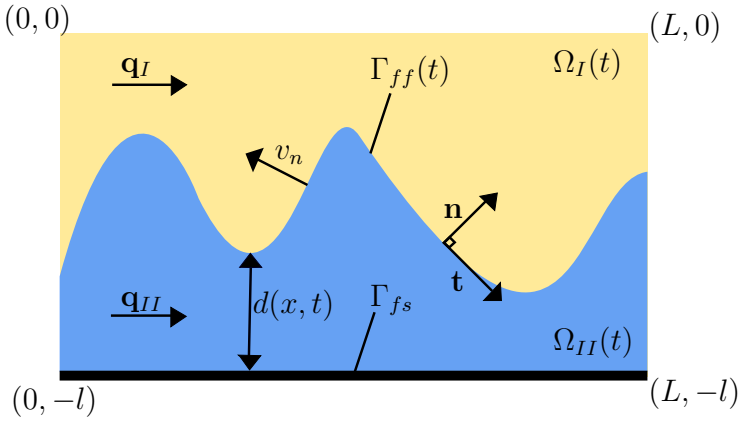

Figure 1: Schematic representation of the lower half of a single pore.

Let $t > 0$ be the time variable. The thickness of the wetting fluid layer is denoted by $d(x,t)$, where $0 \leq d(x,t) \leq l$. The void space consists of two domains. The domain occupied by the non-wetting fluid (fluid-I) and by the wetting (fluid-II) fluid are denoted by respectively

$$\Omega_I(t) := \{(x,y) \in \mathbb{R}^2 | 0 < x < L, -l + d(x,t) < y < 0\},$$
$$\Omega_{II}(t) := \{(x,y) \in \mathbb{R}^2 | 0 < x < L, -l < y < -l + d(x,t)\}.$$

The fluid-fluid interface and the fluid-solid interface are respectively

$$\Gamma_{ff}(t) := \{(x,y) \in \mathbb{R}^2 | 0 < x < L, y = -l + d(x,t)\},$$
$$\Gamma_{fs} := \{(x,y) \in \mathbb{R}^2 | 0 < x < L, y = -l\}.$$

The velocity vectors are denoted by $\mathbf{q}_\alpha = \left(q_\alpha^{(1)}, q_\alpha^{(2)}\right)$, where the index $\alpha = I, II$ is distinguishing between the non-wetting and the wetting fluid, respectively.

Since $d(x,t)$ gives the location of the fluid-fluid interface, the unit normal vector on the fluid-fluid interface pointing into fluid-I and the unit tangent vector are

$$\mathbf{n} := (-\partial_x d, 1)^T / \sqrt{1 + (\partial_x d)^2}, \text{ and } \mathbf{t} := (1, \partial_x d)^T / \sqrt{1 + (\partial_x d)^2}.$$

Given a point $(x, -l + d(x,t))$ on $\Gamma_{ff}(t)$, its normal velocity is

$$v_n := \partial_t d / \sqrt{1 + (\partial_x d)^2}. \tag{1}$$

2.2. Equations in the pore domain

We refer to [58] and assume that the flow of the two fluids is governed by the Navier-Stokes equations

$$\begin{aligned} \rho_\alpha \partial_t \mathbf{q}_\alpha + \rho_\alpha (\mathbf{q}_\alpha \cdot \nabla) \mathbf{q}_\alpha &= -\nabla p_\alpha + \mu_\alpha \nabla^2 \mathbf{q}_\alpha, && \text{in } \Omega_\alpha(t) \ (\alpha = I, II), \\ \nabla \cdot \mathbf{q}_\alpha &= 0, && \text{in } \Omega_\alpha(t) \ (\alpha = I, II). \end{aligned}$$

where ρ_α and μ_α are respectively the constant viscosities and densities, and the pressures are p_α.
We assume that one chemical species (solute) is present in fluid-II, its molar concentration being c. Additionally, there is no mass transfer of the solute form fluid-II to fluid-I, hence, the molar concentration of the solute in fluid-I is zero. The solute concentration changes both by diffusion and convection, resulting in

$$\partial_t c + \nabla \cdot (-D \nabla c + \mathbf{q}_{II} c) = 0, \text{ in } \Omega_{II}(t),$$

where D is the constant diffusion coefficient.

2.3. Boundary conditions at the fluid-fluid interface $\Gamma_{ff}(t)$

Here, we specify the boundary conditions at $\Gamma_{ff}(t)$. This means that all equations in this section are valid only at points at $\Gamma_{ff}(t)$. Firstly, we assume that the velocities of the two fluids are equal at $\Gamma_{ff}(t)$,

$$\mathbf{q}_I = \mathbf{q}_{II}.$$

Secondly, we assume that the normal velocity of $\Gamma_{ff}(t)$ as given in (1), equals the normal velocities of the two fluids,

$$\mathbf{q}_\alpha \cdot \mathbf{n} = v_n \ (\alpha = I, II).$$

Further conditions at $\Gamma_{ff}(t)$ are involving the stress tensors

$$\mathbf{T}_\alpha := -p_\alpha \mathbf{I} + \mu_\alpha \left((\nabla \mathbf{q}_\alpha) + (\nabla \mathbf{q}_\alpha)^T \right) \ (\alpha = I, II),$$

the curvature of $\Gamma_{ff}(t)$

$$\nabla \cdot \mathbf{n} := -\partial_x \left(\frac{\partial_x d}{\sqrt{1 + (\partial_x d)^2}} \right),$$

and the surface tension γ. If γ is affected by the presence of the solute present in fluid-II, one has $\gamma = \gamma(c)$. For example, in [59] the following law is proposed

$$\gamma(c) = \gamma_{ref} \left(1 - b \, \ln \left(\frac{c}{a \, c_{ref}} + 1 \right) \right), \tag{2}$$

where a, b are constants and γ_{ref} is the surface tension at reference concentration c_{ref}. Its tangential stress gradients is

$$\nabla_s \gamma(c) := \nabla \, \gamma(c) - \mathbf{n} \, (\mathbf{n} \cdot \nabla \, \gamma(c)) \, .$$

With this, the third boundary condition at $\Gamma_{ff}(t)$ reads (see [60])

$$(\mathbf{T}_I - \mathbf{T}_{II}) \cdot \mathbf{n} = \gamma(c) \; (\nabla \cdot \mathbf{n}) \; \mathbf{n} - \nabla_s \, \gamma(c).$$

This jump can be written in terms of the normal and the tangential components. At $\Gamma_{ff}(t)$, for the normal component, one has

$$\Big((\mathbf{T}_I - \mathbf{T}_{II}) \cdot \mathbf{n} \Big) \cdot \mathbf{n} = \gamma(c) \; (\nabla \cdot \mathbf{n}) \, ,$$

while for the tangential component, also known as Marangoni stress, one gets

$$\Big((\mathbf{T}_I - \mathbf{T}_{II}) \cdot \mathbf{n} \Big) \cdot \mathbf{t} = -\mathbf{t} \cdot \nabla \, \gamma(c).$$

Finally, the mass balance for the solute at $\Gamma_{ff}(t)$ reads

$$(-D \nabla c + \mathbf{q}_{II} c) \cdot \mathbf{n} = v_n \, c.$$

2.4. Boundary conditions at the fluid-solid interface Γ_{fs}

As before, the equations hold only at the fluid-solid interface Γ_{fs}, where first no-slip is assumed,

$$\mathbf{q}_{II} = \mathbf{0}.$$

For the solute concentration, the normal flux into the solid matrix is zero,

$$(-D \nabla c + \mathbf{q}_{II} c) \cdot \mathbf{n} = 0.$$

2.5. Pore-scale model for the two-phase flow with solute-dependent surface tension

Recall that the sub-domain occupied by fluid α is time dependent, $\Omega_\alpha(t)$, and that the freely moving fluid-fluid interface is $\Gamma_{ff}(t)$ and considering the discussion above, one has

$$\rho_\alpha \partial_t \mathbf{q}_\alpha + \rho_\alpha \left(\mathbf{q}_\alpha \cdot \nabla\right) \mathbf{q}_\alpha = -\nabla p_\alpha + \mu_\alpha \nabla^2 \mathbf{q}_\alpha, \qquad \text{in } \Omega_\alpha(t) \ \ (\alpha = I, II)\,, \tag{3}$$

$$\nabla \cdot \mathbf{q}_\alpha = 0, \qquad \text{in } \Omega_\alpha(t) \ \ (\alpha = I, II)\,, \tag{4}$$

$$\partial_t c + \nabla \cdot (-D\nabla c + \mathbf{q}_{II} c) = 0, \qquad \text{in } \Omega_{II}(t), \tag{5}$$

$$\mathbf{q}_I = \mathbf{q}_{II}, \qquad \text{at } \Gamma_{ff}(t), \tag{6}$$

$$\mathbf{q}_\alpha \cdot \mathbf{n} = v_n, \qquad \text{at } \Gamma_{ff}(t) \ \ (\alpha = I, II)\,, \tag{7}$$

$$\Big(\big(\mathbf{T}_I - \mathbf{T}_{II}\big) \cdot \mathbf{n}\Big) \cdot \mathbf{n} = \gamma(c) \ \ (\nabla \cdot \mathbf{n})\,, \qquad \text{at } \Gamma_{ff}(t), \tag{8}$$

$$\Big(\big(\mathbf{T}_I - \mathbf{T}_{II}\big) \cdot \mathbf{n}\Big) \cdot \mathbf{t} = -\mathbf{t} \cdot \nabla \gamma(c), \qquad \text{at } \Gamma_{ff}(t), \tag{9}$$

$$(-D\nabla c + \mathbf{q}_{II} c) \cdot \mathbf{n} = v_n \, c, \qquad \text{at } \Gamma_{ff}\,(t)\,, \tag{10}$$

$$\mathbf{q}_{II} = \mathbf{0}, \qquad \text{at } \Gamma_{fs}, \tag{11}$$

$$(-D\nabla c + \mathbf{q}_{II} c) \cdot \mathbf{n} = 0, \qquad \text{at } \Gamma_{fs}. \tag{12}$$

2.6. Pore-scale model for the two-phase flow with constant surface tension

Whenever the surface tension is constant, as happening e.g. in the absence of a solute in fluid-II, the tangential components of the normal stresses are equal at $\Gamma_{ff}\,(t)$. In this case, the pore-scale model is simpler, as (5), (10) and (12) become superfluous, while $\gamma(c) = \gamma$ in (8) and (9) reduces to

$$\Big(\big(\mathbf{T}_I - \mathbf{T}_{II}\big) \cdot \mathbf{n}\Big) \cdot \mathbf{n} = \gamma \ \ (\nabla \cdot \mathbf{n})\,, \qquad \text{at } \Gamma_{ff}(t),$$

$$\Big(\big(\mathbf{T}_I - \mathbf{T}_{II}\big) \cdot \mathbf{n}\Big) \cdot \mathbf{t} = 0, \qquad \text{at } \Gamma_{ff}(t).$$

The remaining equations are the same as in Section 2.5.

2.7. Pore-scale model for the unsaturated flow with constant surface tension

A further simplification is to assume that the pressure in the fluid-I is constant and that its mobility is infinite. Essentially, this means that fluid-I plays no role for the flow of fluid-II. This situation appears e.g. if fluid-I is air and is connected to the atmosphere. Then the number of variables reduces to those corresponding to fluid-II. Moreover, we assume the solute is absent in fluid-II, and the surface tension is constant. In this case, (5), (10) and (12) are excessive. Moreover, the model equations in Section 2.5 are further simplified by giving up the equations for $\alpha = I$, reducing to the Navier-Stokes equations in $\Omega_{II}(t)$. At $\Gamma_{ff}(t)$, (7) is valid for $\alpha = II$, and (8), (9) shortens to

$$(\mathbf{T}_{II} \cdot \mathbf{n}) \cdot \mathbf{n} = -\gamma \ \ (\nabla \cdot \mathbf{n})\,, \qquad \text{at } \Gamma_{ff}(t),$$

$$(\mathbf{T}_{II} \cdot \mathbf{n}) \cdot \mathbf{t} = 0, \qquad \text{at } \Gamma_{ff}(t).$$

3. The non-dimensional model equations

To identify the model components that have a larger or smaller impact than others, we first bring the model to a non-dimensional form. To this aim, we use reference quantities and rescale the dimensional ones as specified in Table 1. In particular, μ_{II} and ρ_{II} are taken as reference viscosity, respectively density. Table 1 introduces two length scales, L and l. In a general porous medium, L would reflect the length scale of the entire medium, where l is the one of a pore. As we let a single pore represent the porous medium, we use the width and the length of the pore as described in Section 2.1. In the same spirit, here we define the non-dimensional number $\epsilon := \frac{l}{L} > 0$, and assume that ϵ is small. Observe now that the x and y coordinates are scaled differently, so that they become both of order 1, $\mathcal{O}(1)$. Based on this, the derivatives change into $\frac{\partial}{\partial \hat{x}} = L\,\frac{\partial}{\partial x}$, $\frac{\partial}{\partial \hat{y}} = \epsilon\, L\,\frac{\partial}{\partial y}$. The non-dimensional gradient is $\hat{\nabla} := \left(\partial_{\hat{x}}, \frac{1}{\epsilon}\partial_{\hat{y}}\right)$ due to the different scaling in x and y-direction.

Table 1: Reference and non-dimensional quantities

Variables	Reference values	Non-dimensional variables
time	t_{ref}	$\hat{t} = t/t_{ref}$
space	$x_{ref} = L,\, y_{ref} = l$	$\hat{x} = x/L,\ \hat{y} = y/l = y/(\epsilon\, L)$
depth of the wetting fluid		$\hat{d}^\epsilon = d/l = d/(\epsilon\, L)$
velocities	$q_{ref} = L/t_{ref}$	$\hat{\mathbf{q}}_I^\epsilon = \mathbf{q}_I/q_{ref},\ \hat{\mathbf{q}}_{II}^\epsilon = \mathbf{q}_{II}/q_{ref}$
densities	$\rho_{ref} = \rho_{II}$	$\hat{\rho}_I = \rho_I/\rho_{II} = 1/N,\ \hat{\rho}_{II} = 1$
pressures	$p_{ref} = \left(L^4\,\rho_{ref}\right) / \left(t_{ref}^2\, l^2\right)$	$\hat{p}_I^\epsilon = p_I/p_{ref},\ \hat{p}_{II}^\epsilon = p_{II}/p_{ref}$
kinematic viscosities	$\mu_{ref} = \left(l^2\, p_{ref}\right)/(L\, q_{ref}) = \mu_{II}$	$\hat{\mu}_I = \mu_I/\mu_{II} = 1/M,\ \hat{\mu}_{II} = 1$
surface tension	γ_{ref}	$\hat{\gamma}(\hat{c}^\epsilon) = \gamma(c)/\gamma_{ref}$, $\hat{\gamma} = \gamma/\gamma_{ref} = 1$, if γ is constant
diffusion coefficient	$D_{ref} = L^2/t_{ref}$	$\hat{D} = D/D_{ref}$
molar concentration	c_{ref}	$\hat{c}^\epsilon = c/c_{ref}$
capillary number		$\mathrm{Ca} = (\mu_{ref}\, q_{ref})/\gamma_{ref}$

Note that the dimensionless parameters M, N appearing in Table 1,

$$M := \mu_{II}/\mu_I,\ N := \rho_{II}/\rho_I,$$

may also depend on ϵ. In this respect, here we restrict to the case $N = 1$, while M is assumed first $\mathcal{O}(1)$, and later the limit $M \to \infty$ is considered to show that the two-phase model reduces to the unsaturated, single-phase one.

In the non-dimensional setting, the pore space occupied by the two fluids is

$$\hat{\Omega}_I^\epsilon(\hat{t}) := \{(\hat{x}, \hat{y}) \in \mathbb{R}^2 | 0 < \hat{x} < 1, -1 + \hat{d}^\epsilon(\hat{x}, \hat{t}) < \hat{y} < 0\}, \tag{13}$$

$$\hat{\Omega}_{II}^\epsilon(\hat{t}) := \{(\hat{x}, \hat{y}) \in \mathbb{R}^2 | 0 < \hat{x} < 1, -1 < \hat{y} < -1 + \hat{d}^\epsilon(\hat{x}, \hat{t}). \tag{14}$$

The fluid-fluid and fluid-solid interfaces become

$$\hat{\Gamma}_{ff}^\epsilon(\hat{t}) := \{(\hat{x}, \hat{y}) \in \mathbb{R}^2 | 0 < \hat{x} < 1, \hat{y} = -1 + \hat{d}^\epsilon(\hat{x}, \hat{t})\},$$
$$\hat{\Gamma}_{fs} := \{(\hat{x}, \hat{y}) \in \mathbb{R}^2 | 0 < \hat{x} < 1, \hat{y} = -1\}.$$

The normal and tangent unit vectors are, respectively

$$\hat{\mathbf{n}}^\epsilon := \frac{\left(-\epsilon\ \partial_{\hat{x}}\hat{d}^\epsilon, 1\right)}{\sqrt{1+\left(\epsilon\ \partial_{\hat{x}}\hat{d}^\epsilon\right)^2}},\ \text{and}\ \hat{\mathbf{t}}^\epsilon := \frac{\left(1, \epsilon\ \partial_{\hat{x}}\hat{d}^\epsilon\right)}{\sqrt{1+\left(\epsilon\ \partial_{\hat{x}}\hat{d}^\epsilon\right)^2}}.$$

The normal velocity becomes

$$\hat{v}_n^\epsilon := \frac{\epsilon\ \partial_{\hat{t}}\hat{d}^\epsilon}{\sqrt{1+\left(\epsilon\ \partial_{\hat{x}}\hat{d}^\epsilon\right)^2}}.$$

The non-dimensional stress tensors are

$$\hat{\mathbf{T}}_{\mathbf{I}}^\epsilon := -\hat{p}_I^\epsilon\ \mathbf{I} + \frac{\epsilon^2}{M}\left\{\left(\hat{\nabla}\hat{\mathbf{q}}_I^\epsilon\right) + \left(\hat{\nabla}\hat{\mathbf{q}}_I^\epsilon\right)^T\right\},\ \hat{\mathbf{T}}_{\mathbf{II}}^\epsilon := -\hat{p}_{II}^\epsilon\ \mathbf{I} + \epsilon^2\left\{\left(\hat{\nabla}\hat{\mathbf{q}}_{II}^\epsilon\right) + \left(\hat{\nabla}\hat{\mathbf{q}}_{II}^\epsilon\right)^T\right\}.$$

3.1. Non-dimensional model for the two-phase flow with solute-dependent surface tension

Substituting the non-dimensional variables into the pore-scale model in Section 2.5, for every $\hat{t} > 0$ the non-dimensional model equations for the two-phase flow model with solute-dependent surface tension become

$$\epsilon^2\ \left(\partial_{\hat{t}}\hat{\mathbf{q}}_I^\epsilon + \left(\hat{\mathbf{q}}_I^\epsilon\cdot\hat{\nabla}\right)\hat{\mathbf{q}}_I^\epsilon\right) + \hat{\nabla}\hat{p}_I^\epsilon - \frac{\epsilon^2}{M}\hat{\nabla}^2\hat{\mathbf{q}}_I^\epsilon = 0, \qquad \text{in } \hat{\Omega}_I^\epsilon(\hat{t}), \tag{15}$$

$$\epsilon^2\left(\partial_{\hat{t}}\hat{\mathbf{q}}_{II}^\epsilon + \left(\hat{\mathbf{q}}_{II}^\epsilon\cdot\hat{\nabla}\right)\hat{\mathbf{q}}_{II}^\epsilon\right) + \hat{\nabla}\hat{p}_{II}^\epsilon - \epsilon^2\hat{\nabla}^2\hat{\mathbf{q}}_{II}^\epsilon = 0, \qquad \text{in } \hat{\Omega}_{II}^\epsilon(\hat{t}), \tag{16}$$

$$\hat{\nabla}\cdot\hat{\mathbf{q}}_\alpha^\epsilon = 0, \qquad \text{in } \hat{\Omega}_\alpha^\epsilon(\hat{t})\ \ (\alpha = I, II), \tag{17}$$

$$\partial_{\hat{t}}\hat{c}^\epsilon - \hat{\nabla}\cdot\left(\hat{D}\hat{\nabla}\left(\hat{c}^\epsilon\right) - \hat{\mathbf{q}}_{II}^\epsilon\hat{c}^\epsilon\right) = 0, \qquad \text{in } \hat{\Omega}_{II}^\epsilon(\hat{t}). \tag{18}$$

The boundary conditions at the fluid-fluid interface are

$$\hat{\mathbf{q}}_I^\epsilon = \hat{\mathbf{q}}_{II}^\epsilon, \qquad \text{at } \hat{\Gamma}_{ff}^\epsilon(\hat{t}), \tag{19}$$

$$\hat{\mathbf{q}}_\alpha^\epsilon\cdot\hat{\mathbf{n}}^\epsilon = \hat{v}_n^\epsilon, \qquad \text{at } \hat{\Gamma}_{ff}^\epsilon(\hat{t})\ \ (\alpha = I, II), \tag{20}$$

$$\left(-\hat{D}\hat{\nabla}\hat{c}^\epsilon + \hat{\mathbf{q}}_{II}^\epsilon\hat{c}^\epsilon\right)\cdot\hat{\mathbf{n}}^\epsilon = \hat{c}^\epsilon\,\hat{v}_n^\epsilon, \qquad \text{at } \hat{\Gamma}_{ff}^\epsilon\left(\hat{t}\right), \tag{21}$$

$$\left(\left(\hat{\mathbf{T}}_{\mathbf{I}}^\epsilon - \hat{\mathbf{T}}_{\mathbf{II}}^\epsilon\right)\cdot\hat{\mathbf{n}}^\epsilon\right)\cdot\hat{\mathbf{n}}^\epsilon = \frac{\epsilon^2}{\mathrm{Ca}}\,\hat{\gamma}\left(\hat{c}^\epsilon\right)\left(\hat{\nabla}\cdot\hat{\mathbf{n}}^\epsilon\right), \qquad \text{at } \hat{\Gamma}_{ff}^\epsilon\left(\hat{t}\right), \tag{22}$$

$$\left(\left(\hat{\mathbf{T}}_{\mathbf{I}}^\epsilon - \hat{\mathbf{T}}_{\mathbf{II}}^\epsilon\right)\cdot\hat{\mathbf{n}}^\epsilon\right)\cdot\hat{\mathbf{t}}^\epsilon = -\frac{\epsilon^2}{\mathrm{Ca}}\left(\hat{\mathbf{t}}^\epsilon\cdot\hat{\nabla}\hat{\gamma}(\hat{c}^\epsilon)\right), \qquad \text{at } \hat{\Gamma}_{ff}^\epsilon\left(\hat{t}\right). \tag{23}$$

At the fluid-solid interface, the boundary conditions are

$$\hat{\mathbf{q}}_{II}^\epsilon = \mathbf{0}, \qquad \text{at } \hat{\Gamma}_{fs}, \tag{24}$$

$$\left(-\hat{D}\hat{\nabla}\hat{c}^\epsilon + \hat{\mathbf{q}}_{II}^\epsilon\hat{c}^\epsilon\right)\cdot\hat{\mathbf{n}}^\epsilon = 0, \qquad \text{at } \hat{\Gamma}_{fs}. \tag{25}$$

At $\hat{y} = 0$ we apply symmetry conditions for all variables.

3.2. Non-dimensional model for the two-phase flow with constant surface tension

Similar to Section 2.6, we consider the case without solute and γ being constant. With $\gamma_{ref} = \gamma$, one gets $\hat{\gamma} = 1$ and (22) and (23) become

$$\left(\left(\hat{\mathbf{T}}^{\epsilon}_{\mathbf{I}} - \hat{\mathbf{T}}^{\epsilon}_{\mathbf{II}}\right) \cdot \hat{\mathbf{n}}^{\epsilon}\right) \cdot \hat{\mathbf{n}}^{\epsilon} = \frac{\epsilon^2}{\mathrm{Ca}} \hat{\nabla} \cdot \hat{\mathbf{n}}^{\epsilon}, \qquad \text{at } \hat{\Gamma}^{\epsilon}_{ff}\left(\hat{t}\right), \tag{26}$$

$$\left(\left(\hat{\mathbf{T}}^{\epsilon}_{\mathbf{I}} - \hat{\mathbf{T}}^{\epsilon}_{\mathbf{II}}\right) \cdot \hat{\mathbf{n}}^{\epsilon}\right) \cdot \hat{\mathbf{t}}^{\epsilon} = 0, \qquad \text{at } \hat{\Gamma}^{\epsilon}_{ff}\left(\hat{t}\right). \tag{27}$$

Further, (18), (21) and (25) are not needed anymore and the remaining equations are the same as in the above section.

3.3. Non-dimensional model for unsaturated flow with constant surface tension

Continuing as in Section 2.7, assuming that fluid-I does not influence the flow of fluid-II and in the absence of solute one ends up with (16), (17), (20) (for $\alpha = II$), (24) and

$$\left(\hat{\mathbf{T}}^{\epsilon}_{II} \cdot \hat{\mathbf{n}}^{\epsilon}\right) \cdot \hat{\mathbf{n}}^{\epsilon} = -\frac{\epsilon^2}{\mathrm{Ca}} \hat{\nabla} \cdot \hat{\mathbf{n}}^{\epsilon}, \qquad \text{at } \hat{\Gamma}^{\epsilon}_{ff}\left(\hat{t}\right), \tag{28}$$

$$\left(\hat{\mathbf{T}}^{\epsilon}_{II} \cdot \hat{\mathbf{n}}^{\epsilon}\right) \cdot \hat{\mathbf{t}}^{\epsilon} = 0, \qquad \text{at } \hat{\Gamma}^{\epsilon}_{ff}\left(\hat{t}\right). \tag{29}$$

4. Asymptotic expansion

We use an asymptotic expansion w.r.t. ϵ to derive transversally averaged upscaled (effective) models at the Darcy scale. Since in this section only the non-dimensional variables are used, for the ease of presentation the hats are suppressed. We use the homogenization ansatz, namely that all variables can be expanded regularly w.r.t. ϵ. We assume that

$$\begin{aligned} p^{\epsilon}_{\alpha}(x,y,t) &= p_{\alpha,0}(x,y,t) + \epsilon p_{\alpha,1}(x,y,t) + \mathcal{O}(\epsilon^2)\ (\alpha = I, II), \\ q^{\epsilon,(k)}_{\alpha}(x,y,t) &= q^{(k)}_{\alpha,0}(x,y,t) + \epsilon q^{(k)}_{\alpha,1}(x,y,t) + \mathcal{O}(\epsilon^2)\ (\alpha = I, II, k = 1,2), \\ c^{\epsilon}(x,y,t) &= c_0(x,y,t) + \epsilon c_1(x,y,t) + \mathcal{O}(\epsilon^2), \\ d^{\epsilon}(x,t) &= d_0(x,t) + \epsilon d_1(x,t) + \mathcal{O}(\epsilon^2). \end{aligned} \tag{30}$$

where $p_{\alpha,j}(x,y,t), q^{(k)}_{\alpha,j}(x,y,t), c_j(x,y,t), d_j(x,t)$ are functions describing the $\mathcal{O}(\epsilon^j)$ order approximation (for $j = 1,2,\cdots$) of the corresponding variables. We will now insert these expansions in the model equations and equate terms of the same order in ϵ to find the transversally averaged equations. We do this for different regimes, and end up with different upscaled models.

4.1. Two-phase flow with solute-dependent surface tension

We start with the model for two-phase flow with solute-dependent surface tension (15)-(25). At this point we assume that M is $\mathcal{O}(1)$ w.r.t. ϵ.

4.1.1. Mass conservation

To derive an effective equation for the mass conservation, we follow the ideas in [48, 44, 47]. Substituting the asymptotic expansion (30) in the mass conservation equation (17) and restricting the writing up to the $\mathcal{O}(\epsilon^0)$ terms gives

$$\frac{1}{\epsilon}\,\partial_y q^{(2)}_{\alpha,0} + \left(\partial_x q^{(1)}_{\alpha,0} + \partial_y q^{(2)}_{\alpha,1}\right) + \mathcal{O}(\epsilon) = 0, \text{ in } \Omega^\epsilon_\alpha(t). \tag{31}$$

To show that $q^{(2)}_{\alpha,0} = 0$ in $\Omega^\epsilon_\alpha(t)$, we use (30) in the kinematic conditions (20) and obtain

$$q^{(2)}_{\alpha,0} + \epsilon\,\left(q^{(2)}_{\alpha,1} - q^{(1)}_{\alpha,0}\,\partial_x d_0 - \partial_t d_0\right) + \mathcal{O}(\epsilon^2) = 0, \text{ at } \Gamma^\epsilon_{ff}(t). \tag{32}$$

The lowest order terms in (31) - (32) give

$$\partial_y q^{(2)}_{\alpha,0} = 0, \text{ in } \Omega^\epsilon_\alpha(t), \text{ and } q^{(2)}_{\alpha,0} = 0, \text{ at } \Gamma^\epsilon_{ff}(t),$$

while (24) and the symmetry condition at $y = 0$ lead to

$$q^{(2)}_{\alpha,0} = 0, \text{ in } \Omega^\epsilon_\alpha(t). \tag{33}$$

To upscale the mass balance for the fluids, we consider a thin segment of the pore space, as sketched in Figure 2.

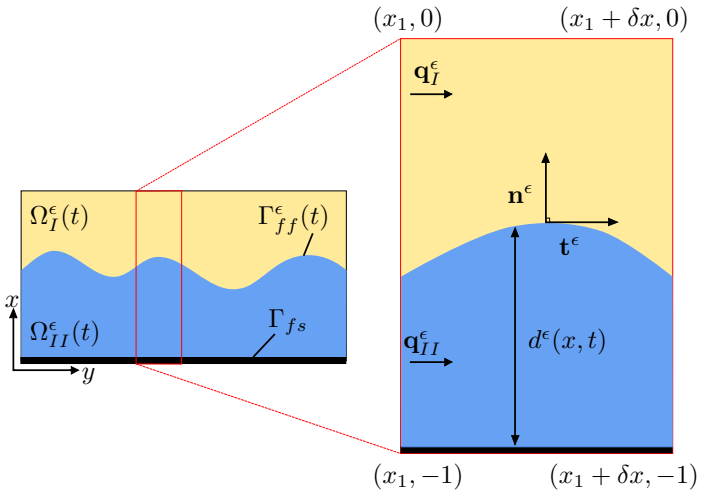

Figure 2: Thin section of the pore space

Let $Y_I := \{(x, y)|x_1 < x < x_1 + \delta x, 0 < y < -1 + d^\epsilon\}$ be the region in this segment that is occupied by fluid-I. By integrating (17) over Y_I, one obtains

$$\int_{Y_I} \nabla \cdot \mathbf{q}^\epsilon_I \, dV_I = 0.$$

In the above equation, we apply the theorem of Gauss and divide all terms by δx, then using (20) and the asymptotic expansions (30) to get

$$\frac{1}{\delta x}\int_{-1+d_0}^{0} q_{I,0}^{(1)}\, dy|_{x=x_1+\delta x} - \frac{1}{\delta x}\int_{-1+d_0}^{0} q_{I,0}^{(1)}\, dy|_{x=x_1} + \frac{1}{\delta x}\int_{x_1}^{x_1+\delta x} q_{I,0}^{(2)}\, dx|_{y=0} - \frac{1}{\delta x}\int_{x_1}^{x_1+\delta x} \partial_t d_0\, dx + \mathcal{O}(\epsilon) = 0.$$

Using (33) and equating the lowest order terms in the above gives

$$\frac{1}{\delta x}\int_{-1+d_0}^{0} \left(q_{I,0}^{(1)}|_{x=x_1+\delta x} - q_{I,0}^{(1)}|_{x=x_1}\right) dy - \frac{1}{\delta x}\int_{x_1}^{x_1+\delta x} \partial_t d_0\, dx = 0.$$

Defining the total flux of fluid-I as

$$\bar{q}_{I,0}^{(1)}(x,t) := \int_{-1+d_0}^{0} q_{I,0}^{(1)}(x,y,t)\, dy, \tag{34}$$

and letting $\delta x \to 0$, one obtains

$$\partial_x \bar{q}_{I,0}^{(1)} - \partial_t d_0 = 0, \text{ for all } 0 < x < 1 \text{ and } t > 0. \tag{35}$$

Similarly using the fluid-II region $Y_{II} := \{(x,y)|x_1 < x < x_1 + \delta x, -1 + d^\epsilon < y < -1\}$, for

$$\bar{q}_{II,0}^{(1)}(x,t) := \int_{-1}^{-1+d_0} q_{II,0}^{(1)}(x,y,t)\, dy, \tag{36}$$

one obtains

$$\partial_x \bar{q}_{II,0}^{(1)} + \partial_t d_0 = 0, \text{ for all } 0 < x < 1 \text{ and } t > 0. \tag{37}$$

Remark 1. *Recalling that the fluids are incompressible, observe that, since d_0 is the thickness of the wetting phase layer in the half-pore, it can be regarded as the saturation of the wetting fluid. In this sense* (35) *and* (37) *are the effective mass balance equations for the two fluid phases.*

4.1.2. Solute transport

To upscale the solute transport, which is needed when considering the Marangoni effect, one uses the asymptotic expansion (30) in (18) to get

$$\begin{aligned} &\partial_t c_0 - \left(\partial_x, \frac{1}{\epsilon}\partial_y\right) \cdot D \left(\partial_x, \frac{1}{\epsilon}\partial_y\right) \left(c_0 + \epsilon c_1 + \epsilon^2 c_2\right) \\ &\quad + \left(\partial_x, \frac{1}{\epsilon}\partial_y\right) \cdot \left(q_{II,0}^{(1)}, q_{II,0}^{(2)} + \epsilon q_{II,1}^{(2)}\right) (c_0 + \epsilon c_1) + \mathcal{O}(\epsilon) = 0, \text{ in } \Omega_{II}^\epsilon(t). \end{aligned} \tag{38}$$

First, we show that c_0 and c_1 do not depend on y. The ϵ^{-2} order term in (38) is leading to

$$\partial_{yy} c_0 = 0, \text{ in } \Omega_{II}^\epsilon(t).$$

From the ϵ^{-1} order term in the boundary conditions (21) and (25), one obtains

$$\partial_y c_0 = 0, \text{ at } \Gamma_{ff}^\epsilon(t) \text{ and } \Gamma_{fs}.$$

This implies that c_0 does not depend on y,

$$c_0 = c_0(x,t), \text{ in } \Omega^{\epsilon}_{II}(t).$$

In a similar fashion, using this, (33), the ϵ^{-1} order term in (38) and ϵ^0 order term in (21), (25), one obtains

$$c_1 = c_1(x,t), \text{ in } \Omega^{\epsilon}_{II}(t).$$

The non-dimensional equation describing the solute concentration (18) can be written as

$$\frac{1}{\epsilon^2}\partial_y\left(D\ \partial_y c^{\epsilon}\right) - \frac{1}{\epsilon}\ \partial_y\left(q^{\epsilon^{(2)}}_{II}\ c^{\epsilon}\right) - \partial_t c^{\epsilon} + \partial_x\left(D\ \partial_x c^{\epsilon} - q^{\epsilon^{(1)}}_{II}\ c^{\epsilon}\right) = 0.$$

We integrate the above equation w.r.t. y from $y=-1$ to $y=-1+d^{\epsilon}$. Applying the Leibniz rule in the last two terms and taking into account that d^{ϵ} depends on x and t, one gets

$$\left[\frac{1}{\epsilon^2}D\partial_y c^{\epsilon} - \frac{1}{\epsilon}q^{\epsilon^{(2)}}_{II}\,c^{\epsilon}\right]_{y=-1}^{y=-1+d^{\epsilon}} - \partial_t\left(\int_{-1}^{-1+d^{\epsilon}} c^{\epsilon}dy\right) + \partial_t d^{\epsilon}c^{\epsilon}|_{y=-1+d^{\epsilon}}$$
$$+\ \partial_x\left(\int_{-1}^{-1+d^{\epsilon}}\left(D\partial_x c^{\epsilon} - q^{\epsilon^{(1)}}_{II}\,c^{\epsilon}\right)dy\right) - \partial_x d^{\epsilon}\left(D\partial_x c^{\epsilon} - q^{\epsilon^{(1)}}_{II}\,c^{\epsilon}\right)|_{y=-1+d^{\epsilon}} = 0.$$

We insert the asymptotic expansion (30) in the above equation, recalling that c_0 and c_1 do not depend on y and that $\partial_y c_2 = 0$ and $q^{(2)}_{II,1} = 0$ at $y=-1$, since $q^{(2)}_{II,0} = 0$ in $\Omega^{\epsilon}_{II}(t)$, one obtains

$$\left(D\partial_y c_2 - q^{(2)}_{II,1}c_0\right)|_{y=-1+d_0} - \partial_t\left(c_0\int_{-1}^{-1+d_0} 1\ dy\right) + \partial_t d_0\ c_0|_{y=-1+d_0}$$
$$+\ \partial_x\left(D\ \partial_x c_0\left(\int_{-1}^{-1+d_0} 1\ dy\right) - c_0\left(\int_{-1}^{-1+d_0} q^{(1)}_{II,0}\ dy\right)\right) - \partial_x d_0\left(D\partial_x c_0 - c_0\ q^{(1)}_{II,0}\right)|_{y=-1+d_0} + \mathcal{O}(\epsilon) = 0.$$

Using (36) and the ϵ order terms from the boundary condition (21) at $y=-1+d_0$, one obtains the effective equation for the solute transport

$$\partial_t\left(c_0\ d_0\right) + \partial_x\left(c_0\ \bar{q}^{(1)}_{II,0}\right) - \partial_x(D\ d_0\ \partial_x c_0) = 0, \text{ for all } 0<x<1 \text{ and } t>0. \tag{39}$$

4.1.3. Momentum conservation

We apply the asymptotic expansion (30) in the horizontal and vertical component of the momentum equation for fluid-II (16). Recalling that $q^{(2)}_{II,0} = 0$, in $\Omega^{\epsilon}_{II}(t)$, for all $t>0$ one has

$$-\partial_{yy}q^{(1)}_{II,0} + \partial_x p_{II,0} - \epsilon\,\partial_{yy}q^{(1)}_{II,1} + \epsilon\,\partial_x p_{II,1} + \mathcal{O}(\epsilon^2) = 0, \tag{40}$$
$$\frac{1}{\epsilon}\ \partial_y p_{II,0} + \partial_y p_{II,1} + \epsilon\ \partial_y p_{II,2} - \epsilon\ \partial_{yy}q^{(2)}_{II,1} + \mathcal{O}(\epsilon^2) = 0. \tag{41}$$

Restricting to ϵ^{-1} order term in (41), for all $0<x<1$ and $t>0$, one gets

$$p_{II,0} = p_{II,0}(x,t).$$

For all $t > 0$, the dominant terms in (40) give

$$\partial_{yy} q^{(1)}_{II,0} = \partial_x p_{II,0}, \text{ in } \Omega^\epsilon_{II}(t). \tag{42}$$

Integrating the above equation in y and taking into account that $p_{II,0}$ is independent of y, we obtain

$$\partial_y q^{(1)}_{II,0} = \partial_x p_{II,0}\, y + A_1(x,t), \text{ in } \Omega^\epsilon_{II}(t), \tag{43}$$

where $A_1(x,t)$ is an integrating constant that will be fixed using boundary condition for $q^{(1)}_{II,0}$. We now assume that the surface tension $\gamma = \gamma(c^\epsilon)$ depends smoothly on the solute concentration. Using (30) and expanding $\gamma(c^\epsilon)$ around c_0 gives

$$\gamma(c^\epsilon) = \gamma\,(c_0) + \epsilon\; c_1\; \gamma'\,(c_0) + \mathcal{O}(\epsilon^2).$$

We apply the asymptotic expansion (30) in the boundary condition (23). Using the above equation and recalling that $q^{(2)}_{\alpha,0} = 0$ at $\Gamma^\epsilon_{ff}(t)$ and that c_0 is independent of y, we get

$$\begin{aligned}
&\frac{1}{\epsilon}\left(\frac{1}{M}\partial_y q^{(1)}_{I,0} - \partial_y q^{(1)}_{II,0}\right) + \left(\frac{1}{M}\partial_y q^{(1)}_{I,1} - \partial_y q^{(1)}_{II,1}\right) + \epsilon\left(\frac{1}{M}\partial_y q^{(1)}_{I,2} - \partial_y q^{(1)}_{II,2}\right)\\
&+ \epsilon\left(\frac{1}{M}\partial_x q^{(2)}_{I,1} - \partial_x q^{(2)}_{II,1}\right) + 2\epsilon\partial_x d_0\left(\frac{1}{M}\partial_y q^{(2)}_{I,1} - \partial_y q^{(2)}_{II,1}\right) - 2\epsilon\partial_x d_0\left(\frac{1}{M}\partial_x q^{(1)}_{I,0} - \partial_x q^{(1)}_{II,0}\right)\\
&- \epsilon\,(\partial_x d_0)^2\left(\frac{1}{M}\partial_y q^{(1)}_{I,0} - \partial_y q^{(1)}_{II,0}\right) + \frac{1}{\mathrm{Ca}}\partial_x\gamma(c_0) + \frac{\epsilon}{\mathrm{Ca}}\partial_x\Big(c_1\gamma'(c_0)\Big) + \mathcal{O}(\epsilon^2) = 0, \text{ at } \Gamma^\epsilon_{ff}(t).
\end{aligned} \tag{44}$$

At this point, the upscaling depends on the capillary number Ca. We will discuss the cases with $\mathrm{Ca} = \epsilon^\beta\,\overline{\mathrm{Ca}}$, for $0 \le \beta \le 3$, where $\overline{\mathrm{Ca}} = \mathcal{O}(1)$. We start by assuming $\mathrm{Ca} = \mathcal{O}(1)$ thus $\beta = 0$. From (44), one gets the tangential stress boundary condition

$$\partial_y q^{(1)}_{II,0} = \frac{1}{M}\,\partial_y q^{(1)}_{I,0}, \text{ at } \Gamma^\epsilon_{ff}(t). \tag{45}$$

Using the above in (43) leads to

$$\frac{1}{M}\,\partial_y q^{(1)}_{I,0}|_{y=-1+d_0} = (-1+d_0)\,\partial_x p_{II,0} + A_1(x,t), \text{ in } \Omega^\epsilon_{II}(t). \tag{46}$$

Applying the asymptotic expansion (30) into (15) and using (33), for all $t > 0$ one has

$$-\frac{1}{M}\,\partial_{yy} q^{(1)}_{I,0} + \partial_x p_{I,0} - \frac{\epsilon}{M}\,\partial_{yy} q^{(1)}_{I,1} + \epsilon\,\partial_x p_{I,1} + \mathcal{O}(\epsilon^2) = 0, \text{ in } \Omega^\epsilon_I(t), \tag{47}$$

$$\frac{1}{\epsilon}\,\partial_y p_{I,0} + \partial_y p_{I,1} + \epsilon\,\partial_y p_{I,2} - \frac{\epsilon}{M}\,\partial_{yy} q^{(2)}_{I,1} + \mathcal{O}(\epsilon^2) = 0, \text{ in } \Omega^\epsilon_I(t). \tag{48}$$

The lowest order term in (48) gives

$$p_{I,0} = p_{I,0}(x,t), \text{ for all } 0 < x < 1. \tag{49}$$

For all $t > 0$, the dominating terms in (47) satisfy

$$\partial_{yy} q^{(1)}_{I,0} = M\,\partial_x p_{I,0}, \text{ in } \Omega^\epsilon_I(t). \tag{50}$$

We integrate the above equation w.r.t. y. We use (49) and the symmetry condition $\partial_y q^{(1)}_{I,0}(x,y,t) = 0$ at $y = 0$, which leads to

$$\partial_y q^{(1)}_{I,0} = M\ \partial_x p_{I,0}\ y, \text{ in } \Omega^\epsilon_I(t). \tag{51}$$

We determine $A_1(x,t)$ from (46), by using (51) at $y = -1 + d_0$, one gets for all $t > 0$

$$\partial_y q^{(1)}_{II,0} = \partial_x p_{II,0}\, y + (-1 + d_0)\left(\partial_x p_{I,0} - \partial_x p_{II,0}\right), \text{ in } \Omega^\epsilon_{II}(t). \tag{52}$$

The lowest order terms in (24) imply that $q^{(1)}_{II,0} = 0$ at $y = -1$. Hence, integrating the above equation in y, one obtains

$$q^{(1)}_{II,0} = \frac{\partial_x p_{II,0}(y^2-1)}{2} + (-1+d_0)\left(\partial_x p_{I,0} - \partial_x p_{II,0}\right)(y+1), \text{ in } \Omega^\epsilon_{II}(t). \tag{53}$$

Integrating the above in y from $y = -1 + d_0$ to $y = -1$ and using (36), yields

$$\bar{q}^{(1)}_{II,0}(x,t) = -\frac{d_0^3}{3}\,\partial_x p_{II,0} - \frac{(1-d_0)\,d_0^2}{2}\,\partial_x p_{I,0}, \text{ for all } 0 < x < 1 \text{ and } t > 0. \tag{54}$$

To derive an effective equation for the velocity of fluid-I, we integrate (51) twice w.r.t. y. To determine the integration constants we use the continuity of the velocity at the fluid-fluid interface. The lowest order terms in (19) imply $q^{(1)}_{I,0} = q^{(1)}_{II,0}$ and hence

$$\bar{q}^{(1)}_{I,0} = -\left[\frac{M\,(1-d_0)^3}{3} + d_0\,(1-d_0)^2\right]\,\partial_x p_{I,0} - \frac{(1-d_0)\,d_0^2}{2}\,\partial_x p_{II,0}, \text{ for all } 0 < x < 1 \text{ and } t > 0. \tag{55}$$

4.1.4. Effect of Ca

We recall that the boundary conditions coming from the normal (22) and the tangential (23) components of the jump in the normal stress depends on the capillary number, Ca. To complete the upscaled model representing the effective behaviour for two-phase flow, we still have to find a relationship between the pressure difference of the fluids (capillary pressure) and the saturation in the porous medium. To this aim, we rewrite (22) as

$$\begin{aligned} &-\frac{1}{\epsilon^2}\,(p^\epsilon_I - p^\epsilon_{II}) + \frac{2}{\epsilon}\,\left(\partial_y q^{\epsilon,(2)}_I - M\,\partial_y q^{\epsilon,(2)}_{II}\right) - (\partial_x d^\epsilon)^2\,(p^\epsilon_I - p^\epsilon_{II}) + 2\,\partial_x d^\epsilon\left(\partial_y q^{\epsilon,(1)}_I - M\,\partial_y q^{\epsilon,(1)}_{II}\right) \\ &- 2\,\epsilon\,\partial_x d^\epsilon\left(\partial_x q^{\epsilon,(2)}_I - M\,\partial_x q^{\epsilon,(2)}_{II}\right) + \frac{\epsilon\,\gamma(c^\epsilon)\,\partial_{xx} d^\epsilon}{\mathrm{Ca}} + \mathcal{O}(\epsilon^2) = 0, \text{ at } \Gamma^\epsilon_{ff}(t). \end{aligned} \tag{56}$$

Whenever $\mathrm{Ca} = \mathcal{O}(1)$ thus $\beta = 0$, applying the asymptotic expansion (30) in the above equation and recalling (33) gives

$$p_{I,0} - p_{II,0} = 0, \text{ for all } 0 < x < 1 \text{ and } t > 0. \tag{57}$$

This means that in the upscaled model the pressures in both phases are equal. Hence the capillary pressure is zero, as commonly assumed in petroleum reservoir simulation models [61]. Since $p_{I,0} = p_{II,0}$ in the pressure relation (57), for simplicity, we set $p_0 = p_{\alpha,0}$ and the effective velocities (54) and (55) become, for all $0 < x < 1$ and $t > 0$

$$\bar{q}^{(1)}_{II,0} = -\frac{d_0^2\,(3-d_0)}{6}\,\partial_x p_0, \tag{58}$$

$$\bar{q}^{(1)}_{I,0} = -\left(\frac{M(1-d_0)^3}{3} + \frac{d_0\,(1-d_0)\,(2-d_0)}{2}\right)\partial_x p_0. \tag{59}$$

Remark 2. *One can recognize* (58) *and* (59) *as the Darcy laws for the two fluid phases. Since* d_0*, respectively* $(1-d_0)$ *are the saturation of the two fluids, the factors multiplying the pressure gradients in these equations can be viewed as relative permeabilities of the two fluids.*

Thus, the upscaled model with $\mathrm{Ca} = \mathcal{O}(1)$ is represented by the mass conservation equations (35), (37), the effective velocities (58), (59) and the solute transport (39). This can be expressed in terms of three primary variables, the saturation of the wetting fluid d_0, the pressure p_0 (recall that the two fluid pressures are equal) and the concentration c_0. Specifically, for all $0 < x < 1$ and $t > 0$ one has

$$\begin{aligned}
\partial_t d_0 + \partial_x \left[\left(\frac{M(1-d_0)^3}{3} + \frac{d_0\,(1-d_0)\,(2-d_0)}{2} \right) \partial_x p_0 \right] &= 0, \\
\partial_t d_0 - \partial_x \left[\frac{d_0^2\,(3-d_0)}{6}\, \partial_x p_0 \right] &= 0, \\
\partial_t\,(c_0\; d_0) + \partial_x \left[c_0 \; \left(\frac{d_0^2\,(3-d_0)}{6} \right) \partial_x p_0 \right] - \partial_x (D\; d_0\; \partial_x c_0) &= 0.
\end{aligned} \tag{60}$$

This means that the surface tension γ plays no role in the effective equations, and therefore the Marangoni effect is lost.

For regimes, where $\mathrm{Ca} = \mathcal{O}(\epsilon^\beta)\ \overline{\mathrm{Ca}}$ with $\beta > 0$, the Marangoni effect will play a role in the upscaled models. For example, if $\mathrm{Ca} = \epsilon\ \overline{\mathrm{Ca}}$ with $\overline{\mathrm{Ca}} = \mathcal{O}(1)$, from (44), one gets the Marangoni stress boundary condition,

$$\partial_y q^{(1)}_{II,0} = \frac{\partial_y q^{(1)}_{I,0}}{M} + \frac{\partial_x \gamma(c_0)}{\overline{\mathrm{Ca}}}, \text{ at } \Gamma^\epsilon_{ff}(t). \tag{61}$$

Using this instead of (45) and repeating the same steps in Section 4.1.3, one gets for $0 < x < 1$ and $t > 0$,

$$\bar{q}^{(1)}_{I,0} = -\left(\frac{M(1-d_0)^3}{3} + \frac{d_0\,(1-d_0)\,(2-d_0)}{2} \right)\, \partial_x p_0 + \frac{(1-d_0)d_0}{\overline{\mathrm{Ca}}}\, \partial_x \gamma(c_0), \tag{62}$$

$$\bar{q}^{(1)}_{II,0} = -\frac{d_0^2\,(3-d_0)}{6}\, \partial_x p_0 + \frac{d_0^2}{2\,\overline{\mathrm{Ca}}}\, \partial_x \gamma(c_0). \tag{63}$$

Remark 3. *Again, one can interpret* (58) *and* (59) *as Darcy laws and identify the related permeabilities. Compared to* (54) *and* (55)*, the Marangoni effect is included.*

The upscaled model is consists of the mass conservation equations (35), (37), effective velocities (62), (63) and the solute transport (39). The model can be expressed in terms of three primary variables, the water saturation d_0, the pressure p_0 (recalling that the two fluid pressures are equal) and the concentration c_0. Specifically, for $0 < x < 1$ and $t > 0$ one has

$$\begin{aligned}
\partial_t d_0 + \partial_x \left[\left(\frac{M(1-d_0)^3}{3} + \frac{d_0\,(1-d_0)\,(2-d_0)}{2} \right) \partial_x p_0 - \frac{(1-d_0)d_0}{\overline{\mathrm{Ca}}}\, \partial_x \gamma(c_0) \right] &= 0, \\
\partial_t d_0 - \partial_x \left[\left(\frac{d_0^2\,(3-d_0)}{6} \right) \partial_x p_0 - \frac{d_0^2}{2\,\overline{\mathrm{Ca}}}\, \partial_x \gamma(c_0) \right] &= 0, \\
\partial_t\,(c_0\; d_0) + \partial_x \left[c_0 \; \left(\frac{d_0^2\,(3-d_0)}{6} \right) \partial_x p_0 \right] - \partial_x (D\; d_0\; \partial_x c_0) &= 0.
\end{aligned} \tag{64}$$

Assuming $\mathrm{Ca} = \epsilon^\beta\ \overline{\mathrm{Ca}}$, with $\beta = 2$ or 3, will lead to different Marangoni stress condition than (61), involving the unknowns c_1, c_2 etc. In this case one needs to find an effective solute transport equation involving c_1, c_2 etc. This is beyond the scope of this paper.

4.2. Two-phase flow with constant surface tension

Now, we consider the pore-scale model in Section 3.2. We begin with the assumption that $M = \mathcal{O}(1)$. We recall that for a constant surface tension, the dynamic boundary conditions are now (26), (27).

4.2.1. Mass conservation

The derivation of the mass conservation equation in this section is identical to the one in Section 4.1.1. The mass conservation equation for the two-phase flow model with constant surface tension is the same as (35) and (37).

4.2.2. Momentum conservation

To derive the effective velocities for fluid-I and fluid-II we can follow the same steps discussed in Section 4.1.3. Since the surface tension γ is constant, we use the continuity in the tangential component of the normal stress (27). It is worth to mention that the capillary number Ca is absent in the tangential stress boundary condition. Applying asymptotic expansion (30) in the boundary condition (27), we get

$$\frac{1}{\epsilon}\left(\frac{1}{M}\partial_y q_{I,0}^{(1)} - \partial_y q_{II,0}^{(1)}\right) + \left(\frac{1}{M}\partial_y q_{I,1}^{(1)} - \partial_y q_{II,1}^{(1)}\right) + \mathcal{O}(\epsilon) = 0, \text{at } \Gamma_{ff}^{\epsilon}(t).$$

The lowest order terms imply

$$\partial_y q_{II,0}^{(1)} = \frac{1}{M}\,\partial_y q_{I,0}^{(1)}, \text{ at } \Gamma_{ff}^{\epsilon}(t),$$

which is same as (45). Further as in Section 4.1.3, one obtains the same effective velocities, (54) and (55).

4.2.3. Effect of Ca

Assuming $\text{Ca} = \epsilon^{\beta}\ \overline{\text{Ca}}$ with $\beta < 3$ and applying asymptotic expansion (30) in (56) (recalling that here $\gamma(c^{\epsilon}) = 1$), the lowest order term implies the same pressure relation as in (57). The upscaled model for the two-phase flow with constant surface tension, large or moderate capillary number can be represented by the mass conservation equations (35), (37), by the effective velocities (59), (58) and the pressure relation (57). This can be expressed in terms of two primary variables, the water saturation d_0 and the pressure p_0 (recall that the two fluid pressures are equal). Specifically, for $0 < x < 1$ and $t > 0$ one has

$$\begin{aligned} \partial_t d_0 + \partial_x\left[\left(\frac{M(1-d_0)^3}{3} + \frac{d_0\,(1-d_0)\,(2-d_0)}{2}\right)\partial_x p_0\right] = 0, \\ \partial_t d_0 - \partial_x\left[\frac{d_0^2\,(3-d_0)}{6}\,\partial_x p_0\right] = 0 \end{aligned} \tag{65}$$

If the capillary number is $\text{Ca} = \epsilon^3\ \overline{\text{Ca}}$, applying (30) in (56), we obtain

$$p_{I,0} - p_{II,0} = \frac{\partial_{xx} d_0}{\overline{\text{Ca}}}. \tag{66}$$

In this case, the upscaled model for the two-phase flow with constant surface tension is given by the mass conservation equations (35), (37), the effective velocities (55), (54) and the capillary pressure relationship (66).

Remark 4. *Observe that compared to traditional two-phase flow models, in which the capillary pressure is a function of the saturation, here this involves second order derivative of the saturation. Here we emphasize the differences between the cases $\beta < 3$ and $\beta = 3$ in the capillary pressure relation* (57) *and* (66)*. In the former, the pressures for both fluids are equal, in other words the capillary pressure is zero. In the later case, one gets a model in which the commonly used pressure-saturation relation is replaced by a differential equation. This is similar to the models in [21, 39]. One can explain the different results in the two cases starting with the observation that γ is the reciprocal of Ca. Thus, in the first case γ is much smaller than in the second case. As in the Young-Laplace equation, the pressure difference is proportional to γ, which whenever small, implies that the two pressure are equal.*

4.2.4. Effect of large viscosity ratio between the fluids

By now we assumed $M = \mathcal{O}(1)$, here we consider $M = \epsilon^{-1}\ \overline{M}$, where $\overline{M} = \mathcal{O}(1)$, which means that the viscosity of fluid-I is much smaller than that of fluid-II. We show that the first order terms when $M \to \infty$, upscaling the equations in Section 4.2 will only include the fluid-II flow whereas the fluid-I flow component is vanishing, reducing the model to the unsaturated flow in Section 4.3. In this respect we first show that the pressure becomes constant (and set as reference value to 0) for fluid-I. Now, considering $M = \epsilon^{-1}\ \overline{M}$ with $\overline{M} = \mathcal{O}(1)$ in (47) and (48), for all $t > 0$ one has

$$\partial_x p_{I,0} + \epsilon\, \partial_x p_{I,1} - \frac{\epsilon}{\overline{M}}\, \partial_{yy} q^{(1)}_{I,0} + \mathcal{O}(\epsilon^2) = 0, \qquad \text{in } \Omega^\epsilon_I(t), \tag{67}$$

$$\frac{1}{\epsilon}\, \partial_y p_{I,0} + \partial_y p_{I,1} + \mathcal{O}(\epsilon) = 0, \qquad \text{in } \Omega^\epsilon_I(t). \tag{68}$$

The lowest order terms in (67) and (68) give

$$\partial_x p_{I,0} = 0, \text{ and } \partial_y p_{I,0} = 0, \text{ in } \Omega^\epsilon_I(t).$$

Hence $p_{I,0}$ is constant in space. We assume it constant in time as well and set this value as a reference zero pressure, implying

$$p_{I,0} = 0, \text{ in } \Omega^\epsilon_I(t).$$

Considering the surface tension constant in (44) and $M = \epsilon^{-1}\ \overline{M}$, where $\overline{M} = \mathcal{O}(1)$, give

$$-\frac{1}{\epsilon}\partial_y q^{(1)}_{II,0} - \partial_y q^{(1)}_{II,1} + \frac{1}{\overline{M}}\partial_y q^{(1)}_{I,0} + \mathcal{O}(\epsilon) = 0, \text{ at } \Gamma^\epsilon_{ff}(t).$$

The ϵ^{-1} order term in the above equation gives

$$\partial_y q^{(1)}_{II,0} = 0, \text{ at } \Gamma^\epsilon_{ff}(t). \tag{69}$$

To find the effective velocity for fluid-II we use (69) instead of (45) when integrating (42) in y. Recalling that γ is constant and $p_{I,0}$ is zero for fluid-I, we follow the same steps as in Section 4.1.3, which results in

$$q^{(1)}_{II,0} = \partial_x p_{I,0}\ \left(\frac{y^2}{2} + (1 - d_0)\ y + \left(\frac{1}{2} - d_0\right)\right), \text{ in } \Omega^\epsilon_{II}(t). \tag{70}$$

Integrating (70) and using (36) gives the Darcy law

$$\bar{q}^{(1)}_{II,0} = -\frac{d_0^3}{3}\ \partial_x p_{II,0}, \text{ for all } 0 < x < 1 \text{ and } t > 0. \tag{71}$$

To find the pressure equation for fluid-II, we take $M = \epsilon^{-1}\,\overline{M}$ in Section 4.1.4 and we use the fact that the pressure for fluid-I is zero. Then the capillary pressure relation in (57) (for $\beta < 3$) changes into

$$p_{II,0} = 0, \text{ for all } 0 < x < 1 \text{ and } t > 0. \tag{72}$$

Remark 5. *Since $p_{II,0} = 0$ in (72), the same holds for $\bar{q}^{(1)}_{II,0}$ in (71) and therefore the saturation is constant in space and time. This is trivial situation corresponding to a steady state.*

Similarly, if $\beta = 3$, (66) becomes

$$p_{II,0} = -\frac{\partial_{xx} d_0}{\overline{\text{Ca}}}, \text{ for all } 0 < x < 1 \text{ and } t > 0. \tag{73}$$

Note that fluid-I plays no role in the upscaled equations, which now reduces to the equations for fluid-II. Specially, the upscaled model consists of the mass conservation equation (37), the effective velocity (71) and the pressure equation (72) (for $\beta < 3$), respectively by (73) (for $\beta = 3$). Hence, in the limit when $M \to \infty$, only the flow of one phase is accounted for the lowest order and the upscaled model for two-phase flow reduces to the upscaled model for the unsaturated flow, as derived in Section 4.3.

4.3. Unsaturated flow with constant surface tension

We here now turn our attention to the model in Section 3.3.

4.3.1. Mass conservation

The derivation of the mass conservation equation in this section is identical to the one in Section 4.1.1. The mass conservation equation for the unsaturated flow model with constant surface tension is the same as (37).

4.3.2. Momentum conservation

We apply the asymptotic expansion (30) in the boundary condition (29) and recall that $q^{(2)}_{II,0} = 0$ at $\Gamma^{\epsilon}_{ff}(t)$, instead of (44), the boundary condition for unsaturated flow at $\Gamma^{\epsilon}_{ff}(t)$ reduces to

$$-\frac{1}{\epsilon}\,\partial_y q^{(1)}_{II,0} - \partial_y q^{(1)}_{II,1} + \mathcal{O}(\epsilon) = 0. \tag{74}$$

The ϵ^{-1} order gives

$$\partial_y q^{(1)}_{II,0} = 0, \text{ at } \Gamma^{\epsilon}_{ff}(t),$$

which is same as in (69). To find the effective velocity for fluid-II, we follow then the same steps as in Section 4.2.4, which results in (71), the same effective law for fluid-II as in Section 4.2.4.

4.3.3. Effects of Ca

In the unsaturated flow case, we disregard fluid-I in (56), which leads to

$$-\frac{1}{\epsilon^2} p^{\epsilon}_{II} + \frac{2}{\epsilon}\,\partial_y q^{\epsilon^{(2)}}_{II} - (\partial_x d^{\epsilon})^2\, p^{\epsilon}_{II} + 2\,\partial_x d^{\epsilon}\,\partial_y q^{\epsilon^{(1)}}_{II} - 2\,\epsilon\,\partial_x d^{\epsilon}\,\partial_x q^{\epsilon^{(2)}}_{II} - \frac{\epsilon\,\gamma(c^{\epsilon})\,\partial_{xx} d^{\epsilon}}{\text{Ca}} + \mathcal{O}(\epsilon^3) = 0, \text{ at } \Gamma^{\epsilon}_{ff}(t).$$

Applying (30) in the above equation and recalling $q^{(1)}_{II,0} = 0$ at $\Gamma^{\epsilon}_{ff}(t)$, we find the same capillary pressure relations as in Section 4.2.4. In particular, for $\beta < 3$, we get (72) and in this case the upscaled model is trivial (see Remark 5). The case Ca$= \epsilon^3\ \overline{\text{Ca}}$ is more interesting as it gives the pressure relation (73). The upscaled model in this case is then represented by (35), (71) and (73). This can be expressed in terms of one primary variable, the water saturation d_0. Specifically, for all $0 < x < 1$ and $t > 0$, one has

$$\partial_t d_0 + \partial_x \left(\frac{d_0^3}{3}\, \frac{\partial_{xxx} d_0}{\overline{\text{Ca}}} \right) = 0, \tag{75}$$

This equation resembles the thin-film lubrication approximation [62]. Moreover, the upscaled models in this section are same as the ones for two-phase flow derived in Section 4.2.4 for the case of a large viscosity ratio.

5. Summary of upscaled models

We recall that in the upscaled models the width of the wetting fluid (fluid-II) d_0 can be seen as its saturation and therefore the saturation of the non-wetting fluid (fluid-I) is $(1 - d_0)$. The effective equations on the Darcy scale are now summarized and discussed in the sections below. These models are obtained in the limit situation when $\epsilon \to 0$. Practically, one has ϵ small but not zero. Therefore the upscaled models should be seen as an approximation of the pore-scale models, having a much simpler structure.

5.1. Two-phase flow with solute-dependent surface tension

If Ca $= \mathcal{O}(1)$, then for all $0 < x < 1$ and $t > 0$, the upscaled model for the pore-scale model (15)-(25) becomes

$$\begin{aligned}
&\partial_t d_0 - \partial_x \bar{q}^{(1)}_{I,0} = 0,\\
&\partial_t d_0 + \partial_x \bar{q}^{(1)}_{II,0} = 0,\\
&\bar{q}^{(1)}_{I,0} + \left(\frac{M(1-d_0)^3}{3} + \frac{d_0\,(1-d_0)\,(2-d_0)}{2} \right) \partial_x p_0 = 0,\\
&\bar{q}^{(1)}_{II,0} + \frac{d_0^2\,(3-d_0)}{6}\, \partial_x p_0 = 0,\\
&\partial_t\,(c_0\, d_0) + \partial_x \left(c_0\, \bar{q}^{(1)}_{II,0} \right) - \partial_x (D\, d_0\, \partial_x c_0) = 0.
\end{aligned} \tag{76}$$

If Ca $= \epsilon\ \overline{\text{Ca}}$, then for all $0 < x < 1$ and $t > 0$, the upscaled counterpart of the pore-scale model in Section 2.5 becomes

$$\begin{aligned}
&\partial_t d_0 - \partial_x \bar{q}^{(1)}_{I,0} = 0,\\
&\partial_t d_0 + \partial_x \bar{q}^{(1)}_{II,0} = 0,\\
&\bar{q}^{(1)}_{I,0} + \left(\frac{M(1-d_0)^3}{3} + \frac{d_0\,(1-d_0)\,(2-d_0)}{2} \right) \partial_x p_0 - \frac{(1-d_0)\,d_0}{\overline{\text{Ca}}}\, \partial_x \gamma(c_0) = 0,\\
&\bar{q}^{(1)}_{II,0} + \frac{d_0^2\,(3-d_0)}{6}\, \partial_x p_0 - \frac{d_0^2}{2\,\overline{\text{Ca}}}\, \partial_x \gamma(c_0) = 0,\\
&\partial_t\,(c_0\, d_0) + \partial_x \left(c_0\, \bar{q}^{(1)}_{II,0} \right) - \partial_x (D\, d_0\, \partial_x c_0) = 0.
\end{aligned} \tag{77}$$

Both upscaled models above are valid for the regimes where the capillary number is either moderate or large, which corresponds to very small surface tension. In particular, if the pressure difference becomes zero, i.e.,

both fluid pressures are equal (here denoted by p_0), the capillary pressure becomes zero as explained in Remark 4. The models in (76) and (77) have a common structure. They both include the mass balance for both fluid phases and the Darcy laws for the two fluid velocities. In terms of porous media models, the factors multiplied by the pressures gradients are representing the relative permeabilities. In (77), the influence of the surface tension gradient, namely the Marangoni effect, is visible. Finally, the last equation gives the mass balance for the solute.

5.2. Two-phase flow with constant surface tension

If solute is not present in the fluid-II phase, the surface tension coefficient is constant. In this case the mass balance for solute is left out. Also, no Marangoni effect is encountered, which simplifies the models. Specifically, assuming $\mathrm{Ca} = \epsilon^{\beta}\ \overline{\mathrm{Ca}}$ with $\overline{\mathrm{Ca}} = \mathcal{O}(1)$ (for $\beta < 3$), the upscaled counterpart of the pore-scale model in Section 2.6 is

$$\begin{aligned}
&\partial_t d_0 - \partial_x \bar{q}^{(1)}_{I,0} = 0,\\
&\partial_t d_0 + \partial_x \bar{q}^{(1)}_{II,0} = 0,\\
&\bar{q}^{(1)}_{I,0} + \left(\frac{M(1-d_0)^3}{3} + \frac{d_0\ (1-d_0)\ (2-d_0)}{2}\right)\partial_x p_0 = 0,\\
&\bar{q}^{(1)}_{II,0} + \frac{d_0^2\ (3-d_0)}{6}\ \partial_x p_0 = 0,
\end{aligned} \tag{78}$$

for all $0 < x < 1$ and $t > 0$. Here the upscaled model is valid in the flow regimes where the capillary number is moderate or large, which implies that the pressures for the two fluid phases are same, as explained in Remark 4. Assuming, $\mathrm{Ca} = \epsilon^{\beta}\ \overline{\mathrm{Ca}}$ with $\overline{\mathrm{Ca}} = \mathcal{O}(1)$ (for $\beta = 3$), the upscaled model becomes

$$\begin{aligned}
&\partial_t d_0 - \partial_x \bar{q}^{(1)}_{I,0} = 0,\\
&\partial_t d_0 + \partial_x \bar{q}^{(1)}_{II,0} = 0,\\
&\bar{q}^{(1)}_{I,0} + \left[\frac{M\ (1-d_0)^3}{3} + d_0\ (1-d_0)^2\right]\ \partial_x p_{I,0} + \frac{(1-d_0)\ d_0^2}{2}\ \partial_x p_{II,0} = 0,\\
&\bar{q}^{(1)}_{II,0} + \frac{d_0^3}{3}\ \partial_x p_{II,0} + \frac{(1-d_0)\ d_0^2}{2}\ \partial_x p_{I,0} = 0,\\
&p_{I,0} - p_{II,0} = \frac{\partial_{xx} d_0}{\overline{\mathrm{Ca}}},
\end{aligned} \tag{79}$$

for all $0 < x < 1$ and $t > 0$. For the upscaled model above, the surface tension cannot be neglected because of the very small capillary number, as mentioned in Remark 4. This is a non-standard model, as it does not express difference of the two fluid pressures as a monotone function of the saturation, but as the second spatial derivative of the saturation. This is in line with [19, 20, 21, 39, 40] (see also the introduction).

5.3. Unsaturated flow with constant surface tension

Continuing in the same spirit as before, for the unsaturated case with constant surface tension in Section 2.7, the upscaled models are simplified. More precisely, assuming $\mathrm{Ca} = \epsilon^{\beta}\ \overline{\mathrm{Ca}}$ with $\overline{\mathrm{Ca}} = \mathcal{O}(1)$, for $\beta < 3$ the upscaled fluid-II pressure becomes zero (as the one for fluid-I) and therefore the flow is vanishing as well.

In this case, the saturation becomes constant in both space and time, which is actually steady state. In this case the upscaled model is trivial. For $\beta = 3$, the upscaled model becomes

$$\begin{aligned} &\partial_t d_0 + \partial_x \bar{q}^{(1)}_{II,0} = 0, \\ &\bar{q}^{(1)}_{II,0} + \frac{d_0^3}{3}\, \partial_x p_{II,0} = 0, \\ &p_{II,0} = -\frac{\partial_{xx} d_0}{\overline{\mathrm{Ca}}} \end{aligned} \tag{80}$$

for all $0 < x < 1$ and $t > 0$. Similar to (79), the upscaled model in (80) is a non-standard model in the sense that the capillary pressure relation is given by the second derivative of the effective saturation. More explanation is in Remark 4. For a large viscosity ratio, the pore-scale model for the two-phase flow in Section 3.2 reduces to the upscaled models in (80).

Remark 6. *The Marangoni effect is only visible for the upscaled model* (77)*. For* (76)*, the Marangoni effect is lost and one immediately sees that* (77) *is equivalent to* (76) *for a constant surface tension. Additionally* (77) *is equivalent to* (78) *for a constant concentration and surface tension. Hence, for the numerical validation in Section 6, we will only consider the three upscaled models* (77)*,* (79) *and* (80)*, as these three models represent the different effective behaviours we have considered.*

6. Model validation

In this section the upscaled models are validated by numerical experiments. Specifically, the full solutions (e.g. $p^\epsilon_\alpha, \mathbf{q}^\epsilon_\alpha, c^\epsilon, d^\epsilon$) of the two-dimensional pore-scale models, computed for pores having different width/length ratios (e.g. $\epsilon = 0.1, 0.07, 0.05, 0.01$), and for different capillary numbers ($\mathrm{Ca}=\epsilon^\beta\ \overline{\mathrm{Ca}}$ with $\overline{\mathrm{Ca}} = \mathcal{O}(1)$, for $\beta = 1, 3$), are averaged in the transversal direction and compared to the approximate upscaled solutions (e.g. $p_{\alpha,0}, \mathbf{q}_{\alpha,0}, c_0, d_0$).

To compute the full solutions of the pore-scale models, we use COMSOL Multiphysics [63]. For the simulations of the upscaled models, we use a simple finite difference scheme on an equidistant mesh, implemented in MATLAB. First and second order central differences are used for the space discretization. For the time discretization, an explicit method with fixed time-step size is used for (77), while for (79) and (80), an implicit method with fixed time-step size is used. We use harmonic averages for the relative permeabilities in the effective flow equations. For the advective flux in (77) we use an upwind approximation. We employ Newton's method for solving the resulting non-linear system of equations.

We specify the pore geometry as in (13) and (14). For (13), we define the inflow and outflow boundaries as

$$\begin{aligned} \Gamma^\epsilon_{I,in}(t) &:= \{(x,y) \in \mathbb{R}^2 | x = 0, -1 + d^\epsilon(0,t) < y < 0\}, \\ \Gamma^\epsilon_{I,out}(t) &:= \{(x,y) \in \mathbb{R}^2 | x = 1, -1 + d^\epsilon(1,t) < y < 0\}. \end{aligned}$$

For (14), the inflow and outflow boundaries are given by

$$\begin{aligned} \Gamma^\epsilon_{II,in}(t) &:= \{(x,y) \in \mathbb{R}^2 | x = 0, -1 < y < -l + d(0,t)\}, \\ \Gamma^\epsilon_{II,out}(t) &:= \{(x,y) \in \mathbb{R}^2 | x = 1, -1 < y < -1 + d^\epsilon(1,t))\}. \end{aligned}$$

In the following, all the presented numerical results are non-dimensional.

6.1. Two-phase flow with solute-dependent surface tension

Here we consider a numerical example of the pore-scale model in Section 3.1 where the regime is $\mathrm{Ca} = \epsilon\ \overline{\mathrm{Ca}}$ with $\overline{\mathrm{Ca}} = 1$. At the fluid-fluid interface, the surface tension coefficient is chosen as (2) with $a = 1$ and $b = 1$, to include the Marangoni effect. The diffusion coefficient is chosen as $D = 1$ and the viscosity ratio as $M = 1$. The initial conditions are

$$d^\epsilon(x, t = 0) = 0.5, \text{ at } \Gamma^\epsilon_{ff}(t = 0),\ c^\epsilon(x, y, t = 0) = 0.25, \text{ in } \Omega^\epsilon_{II}(t = 0),$$
$$\mathbf{q}^\epsilon_\alpha(x, y, t = 0) = \mathbf{0}, \text{ in } \Omega^\epsilon_\alpha(t = 0), \quad p^\epsilon_\alpha(x, y, t = 0) = 0, \text{ in } \Omega^\epsilon_\alpha(t = 0).$$

The inflow and outflow boundary conditions are

$$p^\epsilon_\alpha = 0.023 \text{ at } \Gamma^\epsilon_{\alpha,in}(t), \text{ and } p^\epsilon_\alpha = 0 \text{ at } \Gamma^\epsilon_{\alpha,out}(t),$$
$$c^\epsilon = 1 \text{ at } \Gamma^\epsilon_{II,in}(t), \text{ and } c^\epsilon = 0.25 \text{ at } \Gamma^\epsilon_{II,out}(t).$$

Compatible initial and boundary conditions are chosen by recalling the capillary pressure relation (57). To solve the upscaled model (77), the same initial and boundary conditions are chosen. We use homogeneous Neumann boundary conditions for d_0 at $x = 0$ and $x = 1$. The models are solved for a total time of $t = 0.1$.

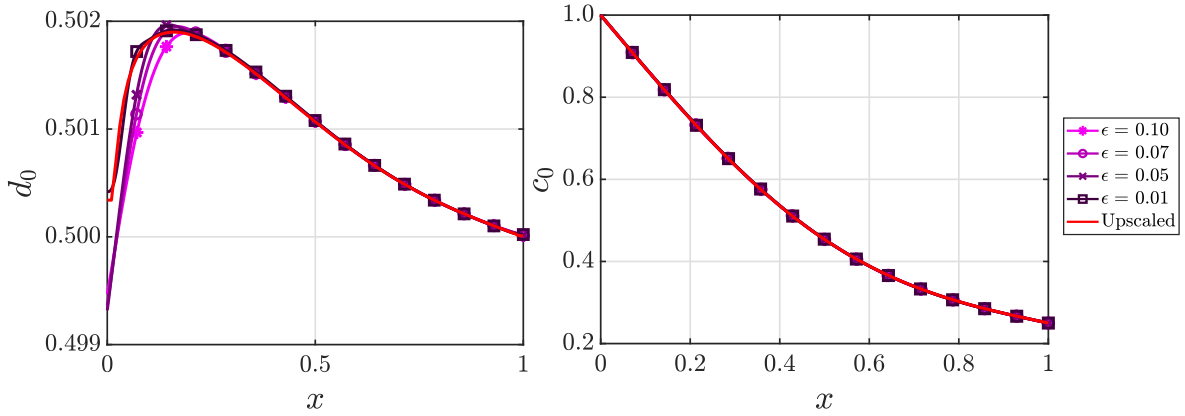

Figure 3: Comparison of the saturation (left) and the concentration (right) of the upscaled model with the transversally averaged solutions of the pore-scale model for different ϵ at $t = 0.1$.

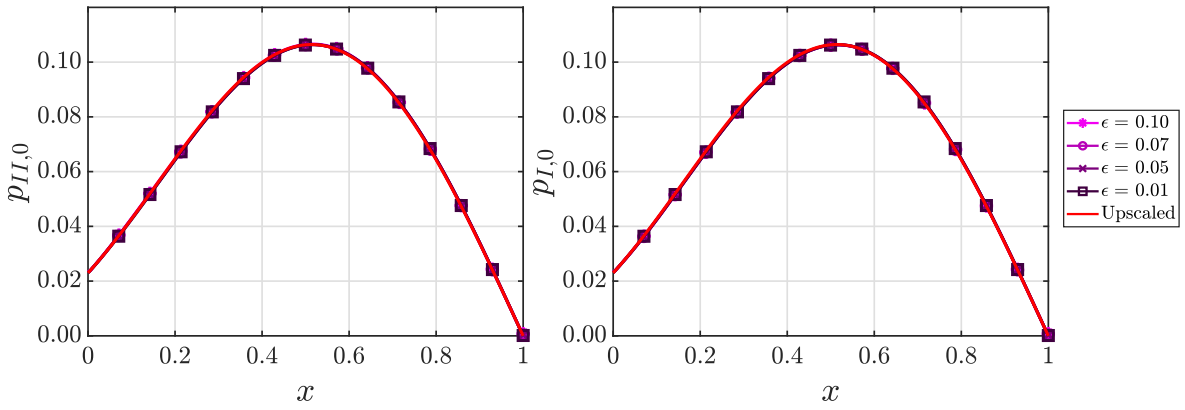

Figure 4: Comparison of the pressures of the wetting (left) and the non-wetting fluid (right) of the upscaled model with the transversally averaged solutions of the pore-scale model for different ϵ at $t = 0.1$.

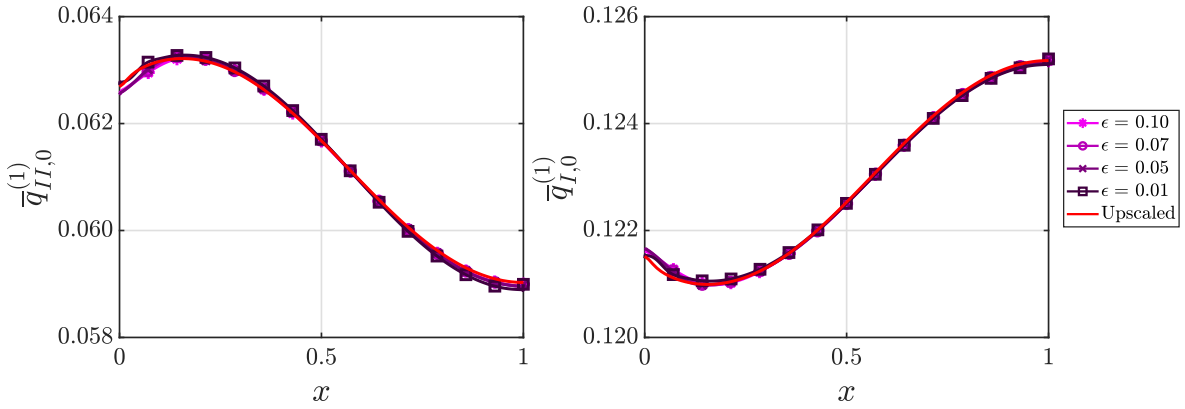

Figure 5: Comparison of the fluxes of the wetting (left) and the non-wetting fluid (right) of the upscaled model with transversally averaged solutions of the pore-scale model for different ϵ at $t = 0.1$.

In Figure 3-Figure 5, we have plotted the upscaled solutions of (77) together with the transversally averaged pore-scale solutions in Section 3.1 for four different ϵ. For decreasing ϵ, the averaged pore-scale solutions are converging to the upscaled solutions.

6.2. Two-phase flow with constant surface tension

Here we consider a numerical example of the pore-scale model in Section 3.2 where the regime is $\mathrm{Ca} = \epsilon^3\ \overline{\mathrm{Ca}}$ with $\overline{\mathrm{Ca}} = 1$. The viscosity ratio is chosen as $M = 1$. The initial conditions are

$$d^\epsilon(x, t = 0) = 0.5 - 1.2\ x + 1.2\ x^2 \text{ at } \Gamma^\epsilon_{ff}(t = 0),$$
$$\mathbf{q}^\epsilon_\alpha(x, y, t = 0) = \mathbf{0},\ p^\epsilon_\alpha(x, y, t = 0) = 0 \text{ in } \Omega^\epsilon_\alpha(t = 0).$$

The inflow and outflow boundary conditions are

$$p_I^\epsilon = 0.023, \text{ at } \Gamma_{I,in}^\epsilon(t), \text{ and } p_I^\epsilon = 0 \text{ at } \Gamma_{I,out}^\epsilon(t),$$
$$p_{II}^\epsilon = -2.377, \text{ at } \Gamma_{II,in}^\epsilon(t), \text{ and } p_{II}^\epsilon = -2.4, \text{ at } \Gamma_{II,out}^\epsilon(t).$$

To avoid a non-smooth behaviour of the fluids, the values chosen above ensures that the initial and the boundary conditions are compatible. Moreover, the capillary pressure relation (66) is also satisfied for $t = 0$. To solve the upscaled model (79), the same initial and boundary conditions are chosen. We use homogeneous Neumann boundary conditions for d_0 at $x = 0$ and $x = 1$. The models are solved for a total time of $t = 1$.

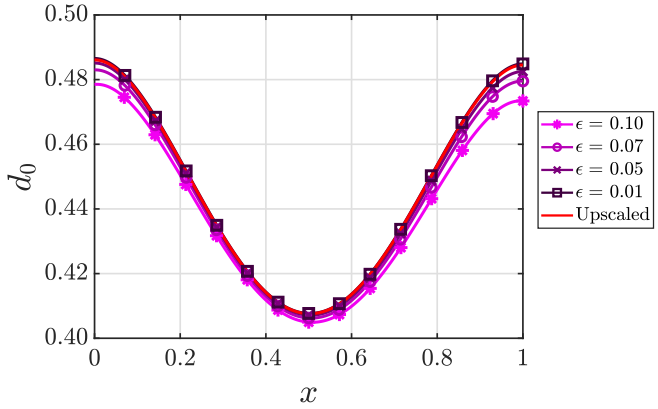

Figure 6: Comparison of the saturation of the wetting fluid of the upscaled model with transversally averaged solutions of the pore-scale model for different ϵ at $t = 1$.

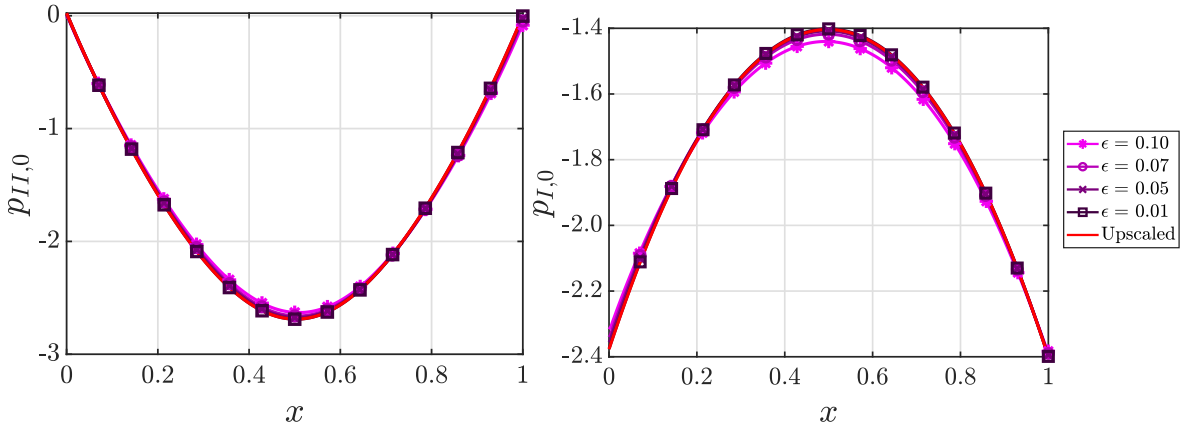

Figure 7: Comparison of the pressures of the wetting (left) and the non-wetting fluid (right) of the upscaled model with transversally averaged solutions of the pore-scale model for different ϵ at $t = 1$.

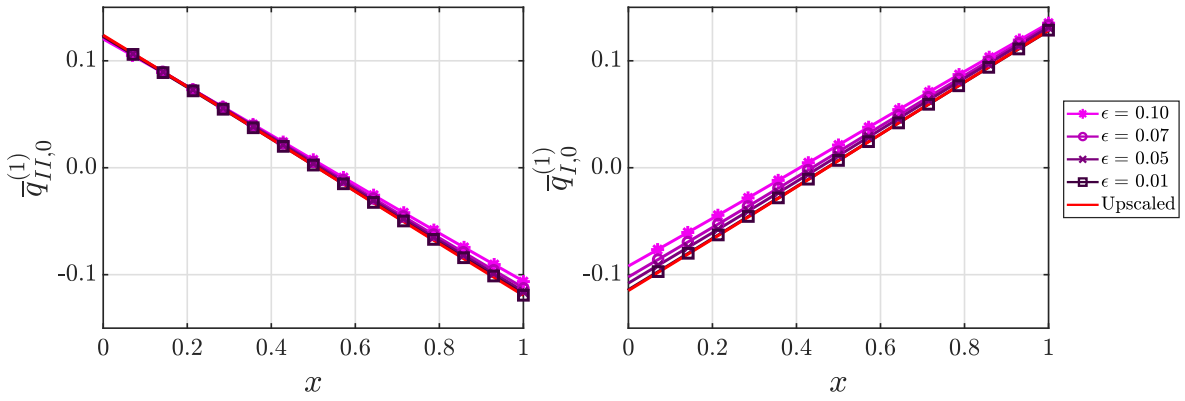

Figure 8: Comparison of the fluxes of the wetting (left) and the non-wetting fluid (right) of the upscaled model with transversally averaged solutions of the pore-scale model for different ϵ at $t = 1$.

In Figure 6 - Figure 8, we have plotted the upscaled solutions of (79) together with the averaged pore-scale solutions in Section 3.2 for various ϵ at $t = 1$. For decreasing ϵ, the averaged pore-scale solutions are converging to the upscaled solutions.

6.3. Unsaturated flow with constant surface tension

The numerical computations of the pore-scale model in Section 3.3 are considered for the regime in $\mathrm{Ca} = \epsilon^3\ \overline{\mathrm{Ca}}$ with $\overline{\mathrm{Ca}} = \mathcal{O}(1)$. The initial conditions are

$$d^\epsilon(x, t = 0) = 0.5 \text{ at } \Gamma^\epsilon_{ff}(t = 0),\ \mathbf{q}^\epsilon_{II}(x, y, t = 0) = \mathbf{0} \text{ in } \Omega^\epsilon_{II}(t = 0),$$
$$p^\epsilon_{II}(x, y, t = 0) = 0 \text{ in } \Omega^\epsilon_{II}(t = 0).$$

The inflow and outflow boundary conditions are

$$p^\epsilon_{II} = 0.023 \text{ at } \Gamma^\epsilon_{II,in}(t) \text{ and } p^\epsilon_{II} = 0 \text{ at } \Gamma^\epsilon_{II,out}(t).$$

The initial conditions and the boundary conditions are same as for the pore-scale model. We use homogeneous Neumann boundary conditions for d_0 at $x = 0$ and $x = 1$. The models are solved for a total time of $t = 1$.

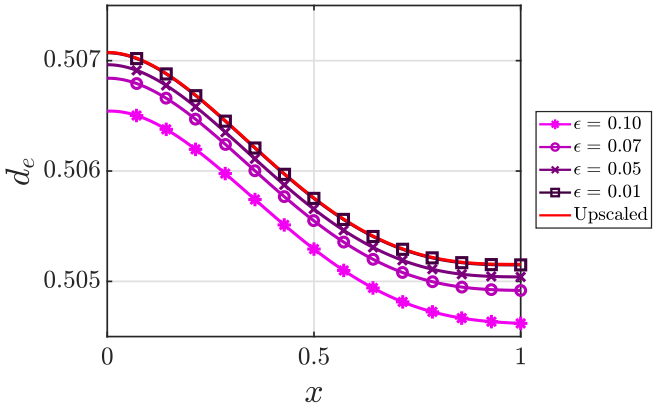

Figure 9: Comparison of the saturation of the wetting fluid of the upscaled model with the transversally averaged solutions of the pore-scale model for different ϵ at time $t = 1$.

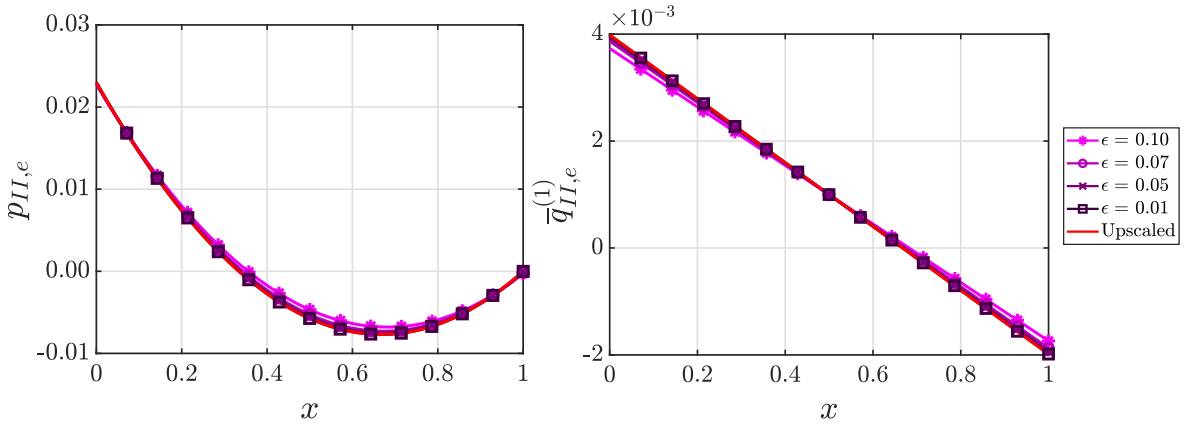

Figure 10: Comparison of the pressure (left) and the flux (right) of the wetting fluid of the upscaled model with the transversally averaged solutions of the pore-scale model for different ϵ at time $t = 1$.

In Figure 9 and Figure 10, we have plotted the upscaled solutions of (80) together with the averaged pore-scale solutions in Section 3.3 for various ϵ at $t = 1$. For decreasing ϵ, the averaged pore-scale solutions are converging to the upscaled solutions.

7. Conclusion

We consider the flow of two immiscible and incompressible phases, respectively the unsaturated flow in a porous medium. We account for the possible dependence of the surface tension on the solute transported by the wetting fluid. For the two-phase flow (the unsaturated, one-phase flow being similar) the starting point is the model at the pore scale, where the two fluids are separated by an interface having an a-priori unknown location but depending on the fluid velocities. The flow is described by the Navier-Stokes equations and

the solute transport by the advection-diffusion equation. At the interface separating the two fluids, relevant interface conditions are imposed. In particular, the difference in the normal stress tensors depend on the surface tension, which may change depending on the solute. Considering a simplified situation, namely a thin strip representing a single pore, we have derived upscaled one-dimensional models describing the averaged behavior of the system. In doing so, different situations are considered, in which the capillary number and the viscosity ratio have a certain behavior w.r.t. the ratio of the pore width and length. In particular, we see that the solute-dependent surface tension (the Marangoni effect) is relevant for the upscaled models only if the capillary number is small enough. Similarly, the capillary pressures effects are lost for low to intermediate capillary numbers, while for larger ones the capillary pressure - saturation dependency is involving a second order derivative of the saturation, as proposed in [20, 21, 39, 40]. Finally, in the case when the viscosity ratio becomes large, the two-phase flow model reduces to the unsaturated, one-phase model.

Although considering a simple geometry, combining asymptotic expansions with various scalings of the non-dimensional parameters show which processes are important at the larger scale and which can be neglected. The upscaling procedure also shows how the capillary pressure depends on the saturation when the capillary pressure should be accounted for. Allowing for other types of fluid displacement, such as a fluid-fluid-solid contact point, and more general geometries open for also other types of upscaled models.

Acknowledgement

The work was supported by the Research Foundation-Flanders (FWO), Belgium through the Odysseus programme (project G0G1316N). We thank the Deutsche Forschungsgemeinschaft (DFG, German Research Foundation) for supporting this work by funding SFB 1313, Project Number 327154368.

References

[1] H. P. G. Darcy, Les Fontaines publiques de la ville de Dijon. Exposition et application des principes à suivre et des formules à employer dans les questions de distribution d'eau, etc, V. Dalamont, 1856.

[2] L. A. Richards, Capillary conduction of liquids through porous mediums, Physics 1 (5) (1931) 318–333. doi:10.1063/1.1745010.

[3] N. R. Morrow, C. C. Harris, Capillary equilibrium in porous materials, SPE Journal 5 (01) (1965) 15–24. doi:10.2118/1011-PA.

[4] R. S. Schechter, J. L. Gidley, The change in pore size distribution from surface reactions in porous media, AIChE Journal 15 (3) (1969) 339–350. doi:10.1002/aic.690150309.

[5] S. Bottero, S. M. Hassanizadeh, P. J. Kleingeld, T. J. Heimovaara, Nonequilibrium capillarity effects in two-phase flow through porous media at different scales, Water Resour. Res. 47. doi:10.1029/2011WR010887.

[6] D. A. DiCarlo, Experimental measurements of saturation overshoot on infiltration, Water Resour. Res. 40 (4). doi:10.1029/2003WR002670.

[7] A. Poulovassilis, Hysteresis of pore water in granular porous bodies, Soil Sci. 109 (1) (1970) 5–12. doi:10.1097/00010694-197001000-00002.

[8] S. Shiozawa, H. Fujimaki, Unexpected water content profiles under flux-limited one-dimensional downward infiltration in initially dry granular media, Water Resour. Res. 40 (7). doi:10.1029/2003WR002197.

[9] L. Zhuang, S. Hassanizadeh, C. J. van Duijn, S. Zimmermann, I. Zizina, R. Helmig, Experimental and numerical studies of saturation overshoot during infiltration into a dry soil, Vadose Zone J. 18 (1). doi:10.2136/vzj2018.09.0167.

[10] R. Glass, T. Steenhuis, J.-Y. Parlange, Mechanism for finger persistence in homogeneous, unsaturated, porous media: theory and verification, Soil science 148 (1) (1989) 60–70. doi:10.1097/00010694-198907000-00007.

[11] F. Rezanezhad, H.-J. Vogel, K. Roth, Experimental study of fingered flow through initially dry sand, Hydrol. Earth Syst. Sci. Discuss. 3 (2006) 2595–2620. doi:10.5194/hessd-3-2595-2006.

[12] E. Abreu, A. Bustos, P. Ferraz, W. Lambert, A relaxation projection analytical-numerical approach in hysteretic two-phase flows in porous media, J. Sci. Comput. 79 (3) (2019) 1936–1980. doi:10.1007/s10915-019-00923-4.

[13] A. Y. Beliaev, R. J. Schotting, Analysis of a new model for unsaturated flow in porous media including hysteresis and dynamic effects, Comput. Geosci. 5 (4) (2001) 345–368.

[14] A. Beliaev, S. Hassanizadeh, A theoretical model of hysteresis and dynamic effects in the capillary relation for two-phase flow in porous media, Transp. Porous Med. 43 (3) (2001) 487–510. doi:10.1023/A:1010736108256.

[15] C. J. van Duijn, K. Mitra, Hysteresis and horizontal redistribution in porous media, Transp. Porous Media 122 (2) (2018) 375–399. doi:10.1007/s11242-018-1009-2.

[16] B. Plohr, D. Marchesin, P. Bedrikovetsky, P. Krause, Modeling hysteresis in porous media flow via relaxation, Comput. Geosci. 5 (3) (2001) 225–256. doi:10.1023/A:1013759420009.

[17] B. Schweizer, Hysteresis in porous media: Modelling and analysis, Interface Free Bound. 19 (3) (2017) 417–447. doi:10.4171/IFB/388.

[18] S. M. Hassanizadeh, W. G. Gray, Thermodynamic basis of capillary pressure in porous media, Water Resour. Res. 29 (10) (1993) 3389–3405. doi:10.1029/93WR01495.

[19] H. Huppert, Flow and instability of a viscous current down a slope, Nature 300 (5891) (1982) 427–429. doi:10.1038/300427a0.

[20] L. Cueto-Felgueroso, R. Juanes, Nonlocal interface dynamics and pattern formation in gravity-driven unsaturated flow through porous media, Phys. Rev. Lett. 101 (24) (2008) 244504. doi:10.1103/PhysRevLett.101.244504.

[21] L. Cueto-Felgueroso, R. Juanes, A phase field model of unsaturated flow, Water Resour. Res. 45. doi:10.1029/2009WR007945.

[22] A. Armiti-Juber, C. Rohde, On the Well-posedness of a Nonlinear Fourth-Order Extension of Richards' Equation, arXiv e-prints (2019) arXiv:1905.07052arXiv:1905.07052.

[23] F. Doster, R. Hilfer, Generalized buckley-leverett theory for two-phase flow in porous media, New J. Phys. 13. doi:10.1088/1367-2630/13/12/123030.

[24] J. Niessner, S. M. Hassanizadeh, A model for two-phase flow in porous media including fluid-fluid interfacial area, Water Resour. Res. 44 (8). doi:10.1029/2007WR006721.

[25] S. M. Hassanizadeh, W. G. Gray, Mechanics and thermodynamics of multiphase flow in porous media including interphase boundaries, Adv. Water Res. 13 (4) (1990) 169–186. doi:10.1016/0309-1708(90)90040-B.

[26] I. S. Pop, C. J. van Duijn, J. Niessner, S. M. Hassanizadeh, Horizontal redistribution of fluids in a porous medium: The role of interfacial area in modeling hysteresis, Adv. Water Resour. 32 (3) (2009) 383–390. doi:10.1016/j.advwatres.2008.12.006.

[27] M. Chapwanya, J. M. Stockie, Numerical simulations of gravity-driven fingering in unsaturated porous media using a nonequilibrium model, Water Resour. Res. 46. doi:10.1029/2009WR008583.

[28] C. J. van Duijn, Y. Fan, L. A. Peletier, I. S. Pop, Travelling wave solutions for degenerate pseudo-parabolic equations modelling two-phase flow in porous media, Nonlinear Anal.-Real World Appl. 14 (3) (2013) 1361–1383. doi:10.1016/j.nonrwa.2012.10.002.

[29] C. J. van Duijn, K. Mitra, I. S. Pop, Travelling wave solutions for the richards equation incorporating non-equilibrium effects in the capillarity pressure, Nonlinear Anal.-Real World Appl. 41 (2018) 232–268. doi:10.1016/j.nonrwa.2017.10.015.

[30] R. Hilfer, F. Doster, P. A. Zegeling, Nonmonotone saturation profiles for hydrostatic equilibrium in homogeneous porous media, Vadose Zone J. 11 (3). doi:10.2136/vzj2012.0021.

[31] A. Lamacz, A. Rätz, S. B., A well-posed hysteresis model for flows in porous media and applications to fingering effects, Adv. Math. Sci. Appl. 21 (2011) 33–64. doi:10.17877/DE290R-6610.

[32] A. Rätz, B. Schweizer, Hysteresis models and gravity fingering in porous media, ZAMM Z. Angew. Math. Mech. 94 (7-8, SI) (2014) 645–654. doi:10.1002/zamm.201200052.

[33] M. Schneider, T. Koeppl, R. Helmig, R. Steinle, R. Hilfer, Stable propagation of saturation overshoots for two-phase flow in porous media, Transp. Porous Media 121 (3) (2018) 621–641. doi:10.1007/s11242-017-0977-y.

[34] H. Zhang, P. Zegeling, A numerical study of two-phase flow models with dynamic capillary pressure and hysteresis, Transp. Porous Media 116 (2) (2017) 825–846. doi:10.1007/s11242-016-0802-z.

[35] M. Graveleau, C. Soulaine, H. Tchelepi, Pore-scale simulation of interphase multicomponent mass transfer for subsurface flow, Transp. Porous Media 120 (2) (2017) 287–308. doi:10.1007/s11242-017-0921-1.

[36] Y. Mehmani, H. Tchelepi, Multiscale computation of pore-scale fluid dynamics: Single-phase flow, J. Comput. Phys. 375 (2018) 1469–1487. doi:10.1016/j.jcp.2018.08.045.

[37] Y. Mehmani, H. Tchelepi, Multiscale formulation of two-phase flow at the pore scale, J. Comput. Phys. 389 (2019) 164–188. doi:10.1016/j.jcp.2019.03.035.

[38] C. Soulaine, H. Tchelepi, Micro-continuum approach for pore-scale simulation of subsurface processes, Transp. Porous Media 113 (3) (2016) 431–456. doi:10.1007/s11242-016-0701-3.

[39] A. Mikelić, On an averaged model for the 2-fluid immiscible flow with surface tension in a thin cylindrical tube, Comput. Geosci. 7 (3) (2003) 183–196. doi:10.1023/A:1025527716078.

[40] A. Mikelic, L. Paoli, On the derivation of the buckley-leverett model from the two fluid navier-stokes equations in a thin domain (vol 1, pg 59, 1997), Comput. Geosci. 4 (1) (2000) 99–101. doi:10.1023/A:1011503731330.

[41] S. Osher, R. P. Fedkiw, Level set methods: an overview and some recent results, journal of Computational physics 169 (2) (2001) 463–502. doi:10.1006/jcph.2000.6636.

[42] H. Abels, H. Garcke, G. Grün, Thermodynamically consistent, frame indifferent diffuse interface models for incompressible two-phase flows with different densities, Math. Models Methods Appl. Sci. 22 (03) (2012) 1150013, 40. doi:10.1142/S0218202511500138.

[43] D. Bresch, Shallow-water equations and related topics, in: Handbook of differential equations: evolutionary equations., Elsevier/North-Holland, Amsterdam, 2009, pp. 1–104. doi:10.1016/S1874-5717(08)00208-9.

[44] C. Bringedal, I. Berre, I. S. Pop, F. A. Radu, A model for non-isothermal flow and mineral precipitation and dissolution in a thin strip, J. Comput. Appl. Math. 289 (2015) 346 – 355. doi:10.1016/j.cam.2014.12.009.

[45] C. Bringedal, I. Berre, I. S. Pop, F. A. Radu, Upscaling of nonisothermal reactive porous media flow under dominant peclet number: The effect of changing porosity, Multiscale Model. Simul. 14 (1) (2016) 502–533. doi:10.1137/15M1022781.

[46] C. Bringedal, I. Berre, I. S. Pop, F. A. Radu, Upscaling of non-isothermal reactive porous media flow with changing porosity, Transp. Porous Media 114 (2) (2016) 371–393. doi:10.1007/s11242-015-0530-9.

[47] K. Kumar, T. L. v. Noorden, I. S. Pop, Effective dispersion equations for reactive flows involving free boundaries at the microscale, Multiscale Model. Simul. 9 (1) (2011) 29–58. doi:10.1137/100804553.

[48] T. L. van Noorden, Crystal precipitation and dissolution in a thin strip, Eur. J. Appl. Math. 20 (1) (2009) 69–91. doi:10.1017/S0956792508007651.

[49] T. L. van Noorden, Crystal precipitation and dissolution in a porous medium: Effective equations and numerical experiments, Multiscale Model. Simul. 7 (3) (2009) 1220–1236. doi:10.1137/080722096.

[50] R. Schulz, Crystal precipitation and dissolution in a porous medium: evolving microstructure and perforated solid matrix, Special Topics & Reviews in Porous Media: An International Journal 10 (4) (2019) 305–321. doi:10.1615/SpecialTopicsRevPorousMedia.2019029274.

[51] D. Landa-Marbán, G. Bødtker, K. Kumar, I. S. Pop, F. A. Radu, An upscaled model for permeable biofilm in a thin channel and tube, arXiv preprint arXiv:1810.06416.

[52] T. van Noorden, I. S. Pop, A. Ebigbo, R. Helmig, An upscaled model for biofilm growth in a thin strip, Water Resour. Res. 46. doi:10.1029/2009WR008217.

[53] M. Peszynska, A. Trykozko, G. Iltis, S. Schlueter, D. Wildenschild, Biofilm growth in porous media: experiments, computational modeling at the porescale, and upscaling, Adv. in Water Res. 95 (2016) 288–301. doi:10.1016/j.advwatres.2015.07.008.

[54] N. Ray, T. van Noorden, F. A. Radu, W. Friess, P. Knabner, Drug release from collagen matrices including an evolving microstructure, ZAMM Z. Angew. Math. Mech. 93 (10-11) (2013) 811–822. doi:10.1002/zamm.201200196.

[55] N. Ray, T. van Noorden, F. Frank, P. Knabner, Multiscale modeling of colloid and fluid dynamics in porous media including an evolving microstructure, Transp. Porous Media 95 (3) (2012) 669–696. doi:10.1007/s11242-012-0068-z.

[56] R. Schulz, P. Knabner, An effective model for biofilm growth made by chemotactical bacteria in evolving porous media, SIAM J. Appl. Math. 77 (5) (2017) 1653–1677. doi:10.1137/16M108817X.

[57] R. Schulz, Biofilm modeling in evolving porous media with beavers-joseph condition, ZAMM Z. Angew. Math. Mech. 99 (3). doi:10.1002/zamm.201800123.

[58] S. Patankar, Numerical heat transfer and fluid flow, CRC press, 1980.

[59] J. E. Smith, R. W. Gillham, Effects of solute concentration–dependent surface tension on unsaturated flow: Laboratory sand column experiments, Water Resour. Res. 35 (4) (1999) 973–982.

[60] L. G. Leal, Advanced transport phenomena: fluid mechanics and convective transport processes, Vol. 7, Cambridge University Press, 2007.

[61] K. Aziz, A. Settari, Petroleum reservoir simulation, Applied Science Publ. Ltd., London, UK.

[62] A. Oron, S. H. Davis, S. G. Bankoff, Long-scale evolution of thin liquid films, Rev. Mod. Phys. 69 (3) (1997) 931. doi:10.1103/RevModPhys.69.931.

[63] COMSOL Multiphysics® v. 5.4., www.comsol.com, COMSOL AB, Stockholm, Sweden.

UHasselt Computational Mathematics Preprint Series

2020

UP-20-01 *Sohely Sharmin, Carina Bringedal, and Iuliu Sorin Pop*, **Upscaled models for two-phase flow in porous media with evolving interfaces at the pore scale**, 2020

2019

UP-19-17 *C. Bringedal*, **A conservative phase-field model for reactive transport**, 2019

UP-19-16 *D. Landa-Marbán, G. Bødtker, B.F. Vik, P. Pettersson, I.S. Pop, K. Kumar, F.A. Radu*, **Mathematical Modeling, Laboratory Experiments, and Sensitivity Analysis of Bioplug Technology at Darcy Scale**, 2019

UP-19-15 *D. Illiano, I.S. Pop, F.A. Radu*, **An efficient numerical scheme for fully coupled flow and reactive transport in variably saturated porous media including dynamic capillary effects**, 2019

UP-19-14 *S.B. Lunowa, I.S. Pop, and B. Koren*, **A Linear Domain Decomposition Method for Non-Equilibrium Two-Phase Flow Models**, 2019

UP-19-13 *C. Engwer, I.S. Pop, T. Wick*, **Dynamic and weighted stabilizations of the L-scheme applied to a phase-field model for fracture propagation**, 2019

UP-19-12 *M. Gahn*, **Singular limit for quasi-linear diffusive transport through a thin heterogeneous layer**, 2019

UP-19-11 *M. Gahn, W. Jäger, M. Neuss-Radu*, **Correctors and error estimates for reaction-diffusion processes through thin heterogeneous layers in case of homogenized equations with interface diffusion**, 2019

UP-19-10 *V. Kučera, M. Lukáčová-Medvidová, S. Noelle, J. Schütz,*, **Asymptotic properties of a class of linearly implicit schemes for weakly compressible Euler equations**, 2019

UP-19-09 *D. Seal, J. Schütz*, **An asymptotic preserving semi-implicit multiderivative solver**, 2019

UP-19-08 *H. Hajibeygi, M. Bastidas Olivares, M. HosseiniMehr, I.S. Pop, M.F. Wheeler*, **A benchmark study of the multiscale and homogenization methods for fully implicit multiphase ow simulations with adaptive dynamic mesh (ADM)**, 2019

UP-19-07 *J.W. Both, I.S. Pop, I. Yotov*, **Global existence of a weak solution to unsaturated poroelasticity**, 2019

UP-19-06 *K. Mitra, T. Köppl, I.S. Pop, C.J. van Duijn, R. Helmig*, **Fronts in two-phase porous flow problems: effects of hysteresis and dynamic capillarity**, 2019

UP-19-05 *D. Illiano, I.S. Pop, F.A. Radu*, **Iterative schemes for surfactant transport in porous media**, 2019

UP-19-04 *M. Bastidas, C. Bringedal, I.S. Pop, F.A. Radu*, **Adaptive numerical homogenization of nonlinear diffusion problems**, 2019

UP-19-03 *K. Kumar, F. List, I.S. Pop, F.A. Radu*, **Formal upscaling and numerical validation of fractured flow models for Richards' equation**, 2019

UP-19-02 *M.A. Endo Kokubun, A. Muntean, F.A. Radu, K. Kumar, I.S. Pop, E. Keilegavlen, K. Spildo*, **A pore-scale study of transport of inertial particles by water in porous media**, 2019

UP-19-01 *Carina Bringedal, Lars von Wolff, and Iuliu Sorin Pop*, **Phase field modeling of precipitation and dissolution processes in porous media: Upscaling and numerical experiments**, 2019